Geoscience Frontiers 13 (2022) 101289

HOSTED BY

Contents lists available at ScienceDirect

Geoscience Frontiers

journal homepage: www.elsevier.com/locate/gsf

Research Paper

Chemical-Abrasion U-Pb zircon geochronology reveals 150 Myr of partial melting events in the Archean crust of the São Francisco Craton

Lorena Martins [a,*], Cristiano Lana [a], Ariela Mazoz [a], Tiago Novo [b]

[a] Applied Isotope Research Group, Departamento de Geologia, Escola de Minas, Universidade Federal de Ouro Preto, Morro do Cruzeiro, Ouro Preto, MG, 35400-000, Brazil
[b] Universidade Federal de Minas Gerais, Programa de Pós-Graduação em Geologia, IGC-CPMTC, Campus Pampulha, Av. Antônio Carlos 6627, Belo Horizonte, MG, 31270-901, Brazil

ARTICLE INFO

Article history:
Received 28 December 2020
Revised 25 June 2021
Accepted 18 August 2021
Available online 21 August 2021

Keywords:
Archean
São Francisco Craton
Crustal reworking
U-Pb geochronology
Lu-Hf isotopes

ABSTRACT

Field observations and CA-LA-ICP-MS U–Pb zircon ages and Hf isotope compositions obtained from migmatitic orthogneisses and granitoids from the Belo Horizonte Complex, southern São Francisco Craton, indicate a major period of partial melting and production of felsic rocks in the Neoarchean. Our observations show that the complex is an important site for studying partial melting processes of Archean crystalline crust. Much of the complex exposes fine-grained stromatic migmatites that are intruded by multiple leucogranitic veins and sheeted dikes. Both migmatites and leucogranite sheets are crosscut by several phases of granitoid batholiths and small granitic bodies; both of which are closely associated with the host banded gneisses. Chemical abrasion followed by detailed cathodoluminescence imaging revealed a wide variety of zircon textures that are consistent with a long-lived period of partial melting and crustal remobilization. Results of U-Pb and Hf isotopes disclose the complex as part of a much wider crustal segment, encompassing the entire southern part of the São Francisco Craton. Compilation of available U-Pb ages suggests that this crustal segment was consolidated sometime between 3000 Ma and 2900 Ma and that it experienced three main episodes of partial melting before stabilization at 2600 Ma. The partial melting episodes took place between 2750 Ma and 2600 Ma as a result of tectonic accretion and peeling off the lithospheric mantle and lower crust. This process is likely responsible for the emplacement of voluminous potassic granitoids across the entire São Francisco Craton. We believe that the partial melting of Meso-Archean crystalline crust and production of potassic granitoids are linked to a fundamental shift in the tectonics of the craton, which was also responsible for the widespread intrusion of large syenitic bodies in the northern part of the craton, and the construction of layered mafic–ultramafic intrusions to the south of the BHC.

1. Introduction

As one of South America's oldest surviving fragments of continental lithosphere, the São Francisco Craton (SFC) is a valuable archive for understanding the nature and origin of the Archean continents (Herz, 1970; Teixeira and Figueiredo, 1991; Machado et al., 1992, 1996; Machado and Carneiro, 1992; Teixeira et al., 1996, 2000; Bastos-Leal et al., 2003; Barbosa et al., 2013). U-Pb zircon crystallization ages in the range of 3500 Ma to 3700 Ma make this craton one of the oldest pieces of continental crust on Earth, and an ideal natural laboratory to investigate tectonic processes leading to Earth's initial geodynamics (Barbosa and Sabaté, 2004; Oliveira et al., 2020). On the basis of U-Pb geochronology, petrography, and major/trace element geochemistry, previous studies have documented a craton-wide period of potassic granitoid magmatism between 2750 Ma and 2650 Ma, which is closely linked to the stabilization of the crust (Lana et al., 2013; Romano et al., 2013; Farina et al., 2015, 2016; Albert et al., 2016; Aguilar et al., 2017; Martínez-Dopico et al., 2017; Moreno et al., 2017; Simon et al., 2018; Cutts et al., 2019). However, because of the complex nature of the tectonic process that preceded stabilization of the SFC, key information about the timing, duration, and underlying tectonic setting for the partial melting events remains elusive.

Studies in the southern part of the craton relate the potassic granitoid magmatism to a major accretionary process, involving reworking of the older TTG crust and supracrustal (greenstone belt + sedimentary) rocks (Farina et al., 2015; Cutts et al., 2019). This mid/lower crustal event is marked by widespread migmatization, multiple intrusions of potassium-rich crustal melts, and

* Corresponding author.
E-mail address: lorenageologa@gmail.com (L. Martins).

https://doi.org/10.1016/j.gsf.2021.101289

construction of voluminous multi-phase batholiths such as the Florestal, Mamona, Pequi, Piracema, Samambaia, Souza Nochese batholiths (Fig. 1). The batholiths themselves record a complex magmatic structure involving intermingling between partially molten gneiss xenoliths, granite flow structures, domains of granite intrusive sheets (into the host gneiss), and amphibolite rafts hosted within granite (e.g., Farina et al., 2016; Cutts et al., 2019). The extensive nature of the partial melting led to large-scale doming of the basement complexes and formed Archean dome and keel features (e.g., around the Pitangui and Florestal batholiths; Fig. 1; Cutts et al., 2019).

Constraining the duration of the partial melting events (leading to stabilization of the SFC) is largely hampered by the complex nature of the datable high T minerals. Previous studies have shown that titanite and monazite were mostly reset by younger, Rhyacian/Transamazonian (2100–2000 Ma) and Neoproterozoic/Brasiliano (600–500 Ma) events (e.g., Aguilar et al., 2017; Cutts et al., 2019), whereas zircons record a wide range of igneous and metamorphic textures, difficult to interpret given the high level of metamictization (e.g., Lana et al., 2013; Romano et al., 2013; Farina et al., 2016). In fact, intense metamictization and multiple events of Pb loss have limited the utility of zircon to disentangle the different tectonothermal events (e.g., Lana et al., 2013; Romano et al., 2013; Farina et al., 2016). A possible solution to this problem would be to undertake a thorough investigation of the zircon textures after chemical abrasion (CA) (Mattinson, 2005) and detailed cathodoluminescence (CL) imaging. Studies applying CA to complex zircons have demonstrated a relevant improvement in the degree of concordance (Huyskens et al., 2016; Wiemer et al., 2017; Bauer et al., 2020). Other studies (e.g., Crowley et al., 2014) have shown the effectiveness of the chemical abrasion in combination with laser ablation inductively coupled plasma mass spectrometry CA-LA-ICP-MS for U–Pb zircon geochronology.

In Fig. 1, we apply CA-LA-ICP-MS to date zircon from mid-crustal rock samples of the craton, aiming to reveal details of the partial melting events that preceded the cratonic stabilization. We focus on migmatitic orthogneisses and granitoid rocks of the Belo Horizonte Complex (BHC): an extensive segment of crystalline crust exposed in the southern part of the SFC (Fig. 1). The complex is at least 40 km long and 50 km wide and it exposes highly migmatized gneisses, multiple phases of granitic intrusions, and multi-phase granitic batholiths (Fig. 1). Previous studies have shown the BHC as a site for major crustal melting and differentiation, with partial melting events dating as far back as 2840 Ma (Noce, 1995). Despite numerous geochronological investigations in the region (e.g., Carneiro, 1992; Machado et al., 1992; Noce, 1995; Carneiro et al., 1997; Noce et al., 1998, 2000, 2005; Lana et al., 2013; Romano et al., 2013; Farina et al., 2015, 2016; Albert et al., 2016), detailed information regarding geochemistry and isotopic evolution of the complex is limited to a few samples, making it difficult to understand its connection with other basement complexes of the craton. We take advantage of the CA-LA-ICP-MS

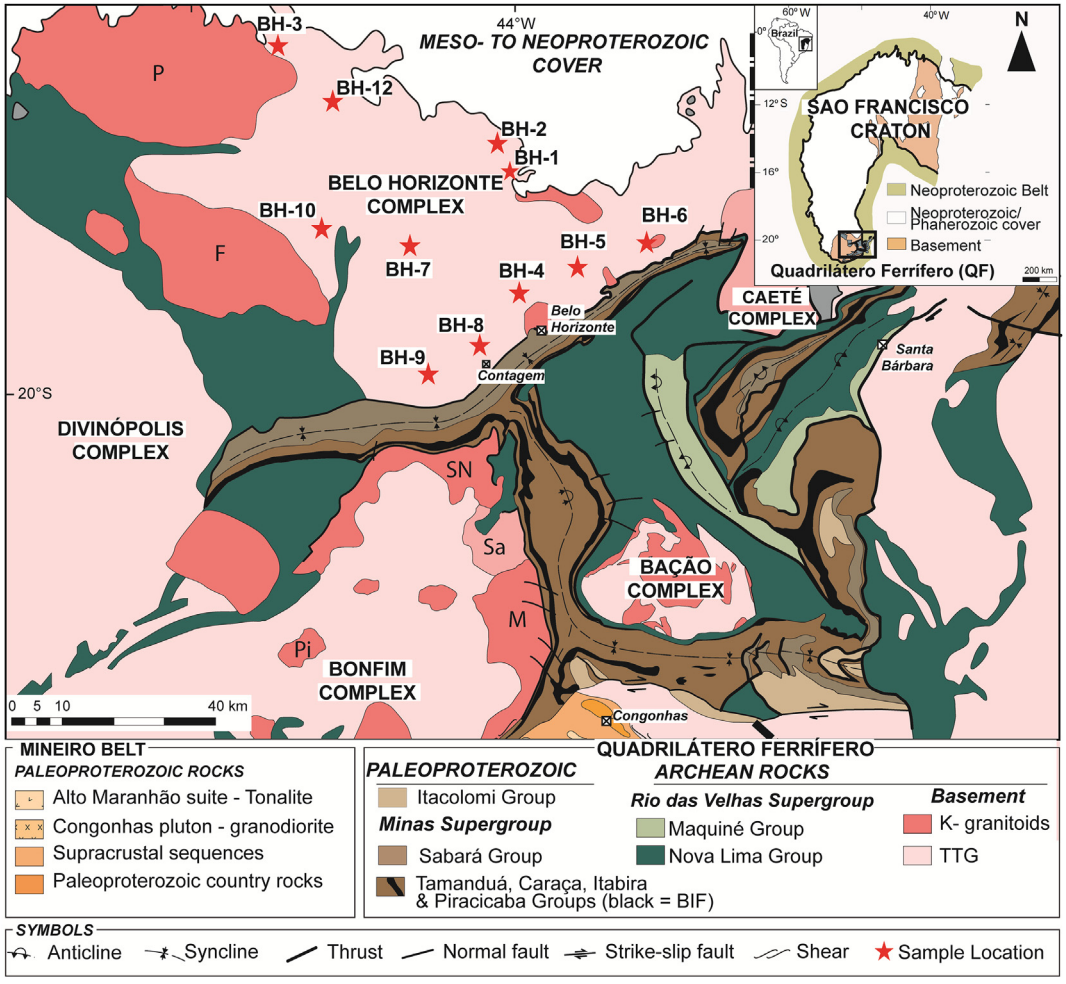

Fig. 1. Geological map of the southern part of the São Francisco Craton, showing in detail the Belo Horizonte Complex and the location of the samples used in this study. Batholith and pluton abbreviations: F–Florestal; M–Mamona; P–Pequi; Pi–Piracema; Sa–Samambaia; SN–Souza Nochese.

technique to investigate in great detail the textural features of approximately 300 zircons, and to provide U-Pb ages and Hf isotopic data for 15 samples collected throughout the complex. A key aspect of this study is to define with better precision the periods of magmatic accretion and partial melting that finally led to the stabilization of the craton in the late Archean.

2. Geological setting

The São Francisco Craton (SFC) comprises one of the most intensively studied Precambrian terranes in South America (Heilbron et al., 2017). The craton itself is surrounded by Neoproterozoic orogenic belts (Araçuaí, Brasília, Rio Preto, Riacho do Pontal, Sergipano) that developed during the amalgamation of West Gondwana, and is partly covered by Meso/Neoproterozoic and Phanerozoic sedimentary units (Almeida et al., 1981; Ledru et al., 1994; Teixeira et al., 1996, 2000; Alkmim, 2004; Barbosa and Sabaté, 2004; Oliveira et al., 2010; Alkmim and Martins-Neto, 2012).

In the southern part of the SFC, the Archean crust exposes amphibolite-facies granitoid-gneiss complexes (e.g., Bonfim, Belo Horizonte, Bação, Santa Bárbara and Caeté) and polydeformed, low-grade Archean to Proterozoic supracrustal sequences. Some studies suggest that these basement complexes were distinct terranes that amalgamated during accretionary periods known as the Rio das Velhas I, Rio das Velhas II and Mamona (Fig. 2A) (Lana et al., 2013; Farina et al., 2015). Initial accretion of mid to early Archean crustal segments seems to have occurred from 2920 Ma to 2850 Ma during the Rio das Velhas I event. Detailed geochemistry and Hf isotopes revealed that this event witnessed only a minor component of juvenile TTG magmatism (Fig. 2B). Further tectonic accretion of larger continental masses promoted crustal reworking with extensive medium-K calc-alkaline magmatism, during the Rio das Velhas II event (Fig. 2C). This event is linked to the development of volcanoclastic and sedimentary rocks of the main greenstone belt sequences across southern SFC (Fig. 2C) (Moreira et al., 2016).

The RV I and II were followed by consolidation of the accreted blocks into a cratonic shield between 2750 Ma and 2680 Ma, during the Mamona event (Fig. 2D) (Lana et al., 2013; Romano et al., 2013; Farina et al., 2015, 2016; Albert et al., 2016; Moreira et al., 2016) (Fig. 2). Here, intense crustal melting and voluminous potassic granitoids formed a stable crystalline basement onto which large Paleoproterozoic supracrustal sequences were deposited (Romano et al., 2013; Farina et al., 2015, 2016). The P–T paths recorded in basement gneisses and amphibolites are consistent with burial and heating followed by near isothermal decompression between 2775 Ma and 2735 Ma (Cutts et al., 2019). This long-lived period of high-grade metamorphism is supported by unzoned garnets suggesting that the temperature conditions were sustained for at least 20 million years (Cutts et al., 2019). It is during the Mamona event that anatectic melts of mid to lower crustal rocks made their way through the mid crust via dikes and veins,

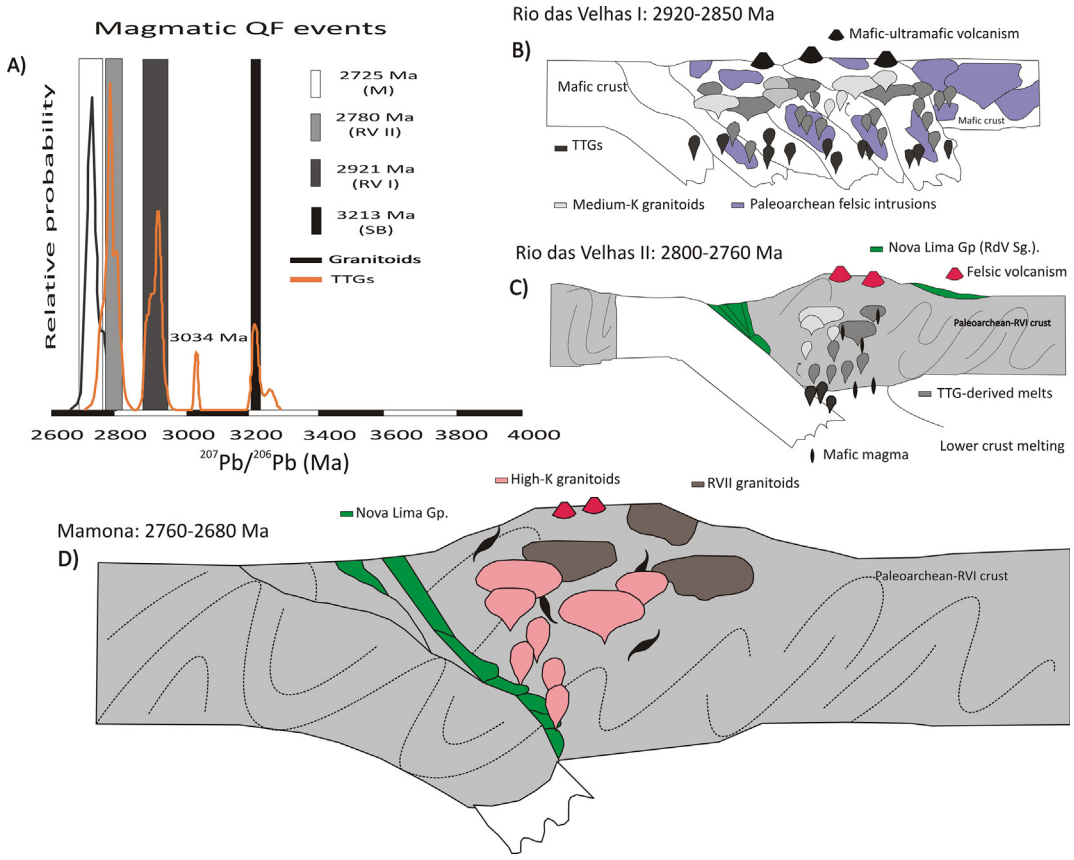

Fig. 2. (A) Compilation of U-Pb data for magmatic zircons in the southern São Francisco Craton. The major peaks of rock crystallization are divided into major periods of magmatic activity known as Santa Barbara (SB), Rio das Velhas I (RVI), Rio das Velhas II (RVII), and Mamona (M) events (modified from Moreira et al., 2016). (B) 2920–2850 Ma Rio das Velhas I event with continental crust formed by multiple additions of TTG magmas and tectonic accretion of mafic and ultramafic rocks (basal units of the Rio das Velhas Supergroup and by greenstone belt remnants around the margin of the Southern São Francisco Craton). (C) Rio das Velhas II event with subduction of an oceanic crust under a continental block and the formation of medium-K granitoids by mixing of different components of the meso-Archean crust. Most of the continental crust formed during the Rio das Velhas II event was produced by reworking older orthogneisses and by partial melting of the mafic oceanic crust. (D) The 2760–2680 Ma Mamona event taking place with tectonic accretion of large and stable continental blocks in the Neoarchean.

and locally formed large batholiths (Romano et al., 2013; Albert et al., 2016). This event also marks a transitional stage between the production of essentially Archean sodic granitoids (2900 Ma to 2800 Ma TTG rocks), and high-potassium calc-alkaline granitoids, which constitute the granite-granodiorite series (Romano et al., 2013; Farina et al., 2015, 2016; Albert et al., 2016). This extensive intracrustal melting was one of the key crustal processes leading to cratonic stabilization (e.g., Laurent et al., 2014; Moyen and Laurent 2018; Nebel et al., 2018).

The basement rocks of the southern SFC expose fine-grained banded gneisses that are intruded by leucogranitic sheets/dikes and large granitoid batholiths (Lana et al., 2013; Romano et al., 2013). Pristine rocks of the TTG series are rare. They have been replaced by medium-potassium rocks during multiple periods of partial melting and granitoid intrusions. Farina et al. (2016) showed that granites and gneisses are all marked by high silica content (70–76 wt.%) and can be subdivided into medium- and high-potassium granitoids. This subdivision is seen by these authors to be a result of the melting of different sources. The medium-potassium rocks bear some similarities with TTG rocks, including high Na_2O, Al_2O_3, and Sr content, low heavy-rare earth content but their overall chemical features suggest mixing between meta-mafic rocks and a component derived by recycling TTG rocks of older continental crust (Farina et al., 2016). Oxygen isotopes data show a secular trend towards high $\delta^{18}O$ (up to 7.79‰) indicating the involvement of metasedimentary rocks in the petrogenesis of the high-K granitoids (Albert et al., 2016). Compilation of Hf data suggests a significant change in the magmatic evolution of the southern SFC at 2.9 Ga; a change that is marked by intense crustal reworking, after a long regime dominated by crustal growth in the Paleoarchean to a Neoarchean (Albert et al., 2016).

Effects of partial melting of the Archean crystalline rocks and high-grade metamorphism are widespread in all the basement complexes of the SFC. Migmatites with a clinopyroxene-bearing assemblage record peak P–T conditions of 5–7 kbar and 700–750 °C (Cutts et al., 2019). The peak conditions are possibly linked to the initial partial melting of crystalline (plus greenstone belt strata) and production of part of the potassic granitoid magma. The peak of granitoid emplacement occurred between 2750 Ma and 2680 Ma with the emplacement of slightly to non-foliated granites as large batholiths (Fig. 1) (Romano et al., 2013) to small leucogranitic veins and dikes.

Apart from basement gneiss complexes, the southern part of the SFC also exposes greenstone belt rocks of the Rio das Velhas Supergroup and Paleoproterozoic supracrustal rocks of the Minas Basin. The Rio das Velhas is a typical Archean greenstone belt, subdivided into Nova Lima and Maquiné Groups (Dorr, 1969). The basal unit (the Nova Lima Group) is a volcano-sedimentary sequence consisting of mafic and ultramafic rocks (basalt–komatiite), and subordinate felsic rocks, as well chemical, clastic and volcanoclastic sedimentary rocks. Felsic volcanic rocks emplaced at 2.79–2.75 Ga mark the final deposition of the Nova Lima Group (Machado et al., 1992, 1996; Schrank and Machado 1996; Noce et al., 2005; Hartmann et al., 2006; Baltazar and Zucchetti, 2007). An association of conglomerates and sandstones characterizes the Maquiné Group, the upper unit of the greenstone belt (Dorr, 1969; Moreira et al., 2016). The Paleoproterozoic Minas Supergroup unconformably overlies the Archean units and comprises passive margin and syn-orogenic sediments, which were deposited after stabilization of the craton (Dorr, 1969; Alkmim and Marshak, 1998; Romano et al., 2013).

3. Field observation

The Belo Horizonte Complex (BHC) is one of the largest crustal segments in the southern part of the SFC (Fig. 1). To the south, east and west the complex is surrounded by mafic to intermediate schist and pelitic rocks of the Nova Lima Group. To the north, the complex is covered by Proterozoic rocks of the Bambuí Group (Babinski et al., 2007; Alkmim and Martins-Neto, 2012). Although the crystalline rocks of the SFC are for most parts buried under thick soil cover and recent sedimentary rocks, several building-stone quarries and railway/road cuts expose the crystalline rocks throughout the region. Field observations show that some 60%–80% of the BHC exposes highly migmatized banded gneisses that are locally intruded by relatively homogenous granitoids (Fig. 1). The banded gneisses are characterized by tightly folded biotite-rich melanocratic, and biotite-free leucocratic bands. Close to the contact with the greenstone rocks to the south (Fig. 1), the migmatitic fabric is completely obscured by extensive partial melting (e.g., diatexite and metatexite) and granitoid intrusion. The largest concentrations of granitoid bodies are often found around the edges of the crystalline complexes, near the contact with the greenstone belt strata.

Results of our field mapping show that the dominant rock type is a grey/pink orthogneiss migmatite, characterized by alternating quartz-feldspathic leucocratic bands and minor cm-wide discontinuous layers of biotite-rich mesocratic bands (Fig. 3a–d). The protolith was likely a TTG rock, which may occur as a foliated biotite gneiss in other parts of the BHC.

In the migmatitic rocks, the leucocratic bands consist of plagioclase, quartz and subordinate feldspar, exhibiting granoblastic textures. The mesocratic bands contain predominantly biotite and feldspar (sometimes phenocrysts or elongated grains), and show lepidoblastic textures. In some places, the migmatite may develop a convoluted aspect, or show a complex structural pattern associated with high volumes of leucogranitic material (leucosome) (Fig. 3b–f). Here, the stromatic texture often gives way to a metatexite or diatexite texture.

As with diatexites described elsewhere (e.g., Carvalho et al., 2016, 2017), the BHC migmatites are marked by abundant schlieren-type textures, which are dominantly dark to light grey and vary in shape and size. They represent melt-rich parts of the regional migmatites that underwent complex heterogeneous magmatic flow. The schlieren diatexite includes scattered remnants of a mafic material derived from sheared/dismembered amphibolite layers (Fig. 3d–f).

The metatexite has a dominant quartz-feldspathic composition and is characterized by high contents of coarse-grained quartz and feldspar and very little biotite (Fig. 3e). The K-feldspar crystals are euhedral and define a framework filled with irregular quartz. Most metatexites occur as small (cm- to m-scale) patches within the diatexite, showing a homogenous texture, larger grain size, and higher quartz and K-feldspar contents than the host diatexite. Although P-T conditions cannot be established because of the type of rocks preserved in the area, the widespread migmatitic textures, the large volumes of granitic melt intruding the gneiss and the features indicative of partial melting are consistent with crustal reworking at mid to lower crustal levels.

Some outcrops show important sub-vertical shear zones associated with small lenticular domains of leucogranite with diffuse margins. Mylonitic shear zones are also common, characterized by quartz ribbons and sigmoidal eye-shaped (augen) porphyroblasts of feldspars enveloped by biotite-rich layers. These shear zones were avoided in this study given evidence of intense fluid

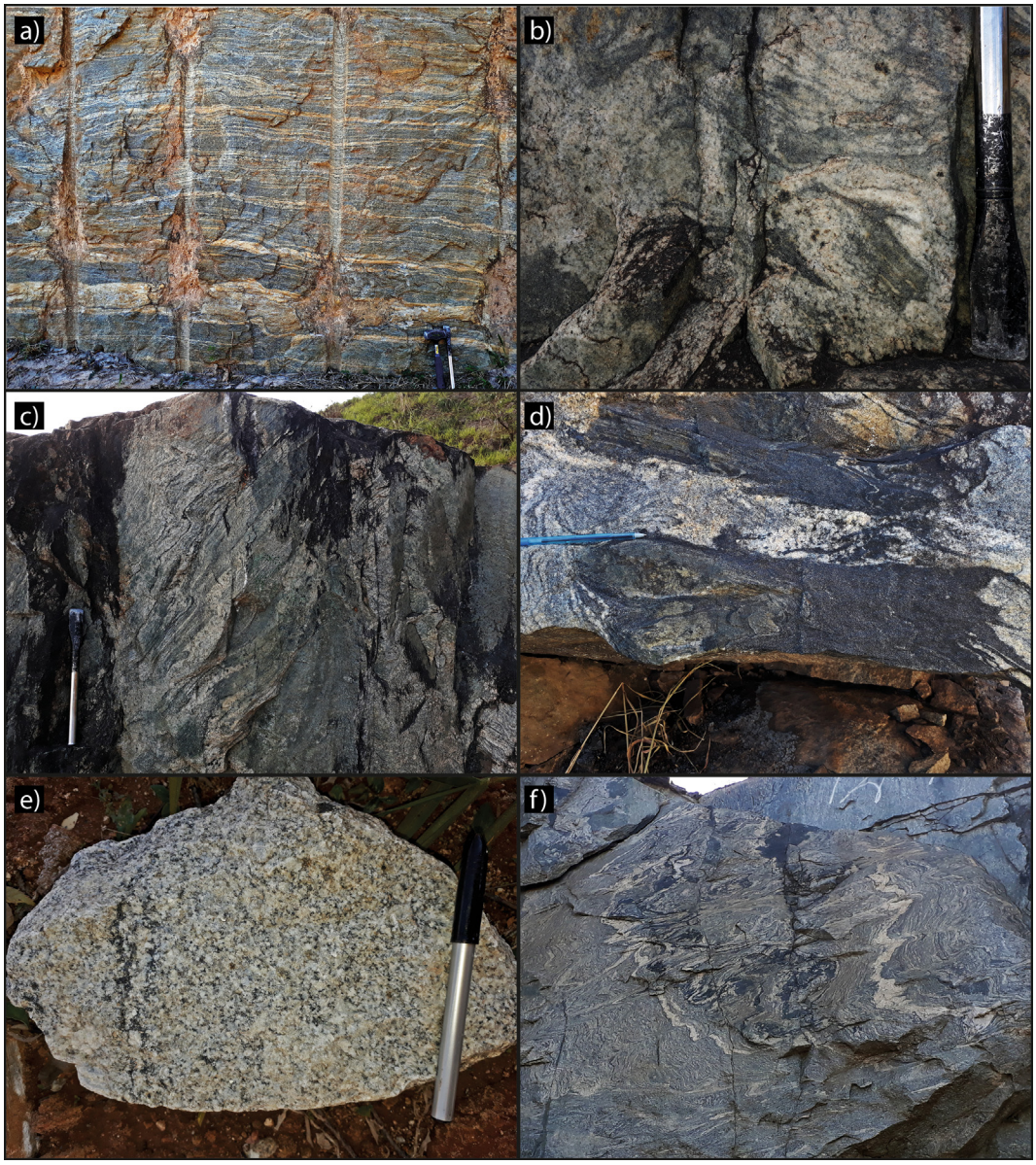

Fig. 3. Field photographs showing the main stages of partial melting of the Archean rocks in the Belo Horizonte Complex. (a) Typical aspect of the stromatic metatexite, in the lower part of the image the migmatite hosts a fine leucogranite layer. (b) Detailed photo of a schlieren diatexite rich in leucosome. (c) Heterogeneous schlieren diatexite with schlieren of biotite and schollen of stromatic migmatite in the granitic leucosome. (d) Dismembered amphibolite dike in diatexite. (e) Detailed photo of a nebulitic diatexite exhibiting medium-grained inequigranular texture. (f) Heterogeneous aspect of the BH migmatite showing felsic, intermediate, and mafic bands.

circulation along the shear planes and hence the unlikelihood of getting geologically meaningful ages from them.

4. Analytical methods

Zircon grains were pretreated before the LA-ICP-MS (Laser Ablation Inductively Coupled Plasma Mass Spectrometry), using chemical abrasion (CA) procedures based on Mattinson (2005). The goal was to isolate zircon domains that have remained closed with respect to U-Pb since crystallization by removing altered, metamict zones. This technique utilizes high-temperature annealing to restore the crystallinity in damaged parts of the zircon crystals, followed by acid leaching that dissolves parts of the crystals where strong radiation damage and most likely Pb loss occurred, at conditions where the crystalline zircon does not dissolve. We note that CA is an empirical approach and there is no guarantee that Pb-loss will be completely eliminated (Huyskens et al., 2016; Wiedmann et al., 2019). For example, at higher leaching temperatures zircons might dissolve entire, while low temperatures will not effectively remove all zones that have lost Pb.

The initial thermal annealing step was carried out in ceramic crucibles in a muffle furnace at 850 °C for 60 h. The selected grains were then placed into sealed Teflon vessels followed by partial dissolution in an acid mixture of 0.8 mL HF $_{(conc)}$ and 3.6 mL 1:1 $HNO_{3(conc)}$ + Milli-Q-H_2O. The experiments were done in 2 steps of 10 min at 175 °C and 60 °C, respectively, using a Milestone EHTOS 1 microwave digestion system at 1500 W (Wiemer et al., 2017). The acid solution (HF-HNO_3) was then pipetted out and the zircon crystals were washed with 3 N HCl for several hours, and repeatedly rinsed with ultrapure Milli-Q water in a centrifuge. The residues were then evaporated on a stove at 100 °C for 12 h. Finally, the chemically abraded grains were mounted in conventional epoxy resin, and then polished to expose their interior.

All CL images were obtained using a scanning electron microscope (JEOL JSM-6510) at the Departamento de Geologia (DEGEO) of the Universidade Federal de Ouro Preto (Brazil). Zircon grains from 15 samples were analyzed for U-Pb. Nine of those samples were later analyzed for Lu-Hf isotopes. U-Pb isotopic concentrations were determined using the ThermoFinnigan Element II, sector field ICP-MS, coupled to a Photon-Machine 193 excimer laser ablation system, at the DEGEO. The analytical spots (20 μm diameter) were ablated in automated mode. The ablated material was transported in He carrier gas mixed with Ar prior to introduction into the ICP-MS. Masses of Pb (^{204}Pb, ^{206} Pb, ^{207}Pb, ^{208}Pb), ^{232}Th, and ^{238}U were measured. Data was collected in peak jumping mode during 20 s and 40 s, for background and sample measurement. Laser conditions were 10 Hz at 4 J/cm^2 fluence. Multiple analyses of reference material GJ-1 reference zircon (608 ± 1 Ma; Jackson et al., 2004) were performed during each analytical session. In addition, multiple analyses of reference zircon 91500 (1065 ± 1; Wiedenbeck et al., 1995) and BB (561 ± 2 Ma; Santos et al., 2017) were used for quality control. The 91500 secondary standard gave Concordia ages of 1064.9 ± 2.2 (2SD, n = 75; MSWD = 2.4). The calculated age is consistent, within uncertainty, with the ID-TIMS value reported by Wiedenbeck et al. (1995). The BB secondary standard gave a concordia age of 562.4 ± 1.3 Ma (2SD, n = 63; MSWD = 1.12). This age is consistent with the ID-TIMS age of 561 ± 2 Ma reported by Santos et al. (2017). The results of the LA-ICP-MS analyses for unknowns and zircon reference materials are presented in Supplementary data Tables S1 and S2. Glitter 4.4.3 software (Van Achterbergh et al., 2001) was used to reduce data. As recommended by (Crowley et al., 2014) our reference materials were treated with chemical abrasion prior to the analyses. Error propagation and Pbc corrections were applied using an in-house spreadsheet (e.g., Farina et al., 2016). All U-Pb concordia diagrams were plotted using Isoplot Excel (Ludwig, 2012). Errors and uncertainties are reported at 2σ, isotope ratios and weighted average ages are reported as weighted means at 95% confidence level.

The Lu-Hf isotopes were measured on a ThermoFinnigan Neptune multi-collector ICP-MS coupled to a Photon-Machine 193 nm ArF excimer laser system, at DEGEO following the methods of Gerdes and Zeh (2006, 2009). Laser spot sizes of 40–50 μm were made on the same zircon domain previously analyzed for U-Pb. Isotopic concentrations were acquired in static mode during the 60 s of ablation. Nitrogen (~0.080 L/min) was introduced into the Ar sample carrier gas via an Aridus nebulization system. ^{172}Yb, ^{173}Yb and ^{175}Lu were measured to correct for ^{176}Yb and ^{176}Lu isobaric interference. The ^{176}Lu and ^{176} Yb were calculated using a ^{176}Lu/^{175}Lu ratio of 0.02658 (J.W. Goethe University of Frankfurt in-house value) and ^{176}Yb/^{173}Yb of 0.796218 (Chu et al., 2002). To validate accuracy and external reproducibility five reference materials were used before and during runs: BB ^{176}Hf/^{177}Hf = 0.2816713 ± 0.0000028 (Santos et al., 2017), GJ-1 ^{176}Hf/^{177}Hf = 0.282000 ± 0.000005 (Morel et al., 2008), Plesovice ^{176}Hf/^{177}Hf = 0.282482 ± 0.000013 (Sláma et al., 2008), Mudtank ^{176}Hf/^{177}Hf = 0.282504 ± 0.000044 (Black and Gulson, 1978; Woodhead and Hergt, 2005), 91500 ^{176}Hf/^{177}Hf = 0.282307 ± 0.000031 (Wiedenbeck et al., 2004) and Temora ^{176}Hf/^{177}Hf = 0.282680 ± 0.000031(Black et al., 2003). Multiple analyses of these reference materials yielded average ^{176}Hf/^{177}Hf ratios of 0.281682 ± 50 (2SD, n = 9), 0.282001 ± 30 (2SD, n = 29), 0.282470 ± 114 (2SD, n = 10), 0.282493 ± 76 (2SD, n = 20), 0.282 280 ± 56 (2SD, n = 19), and 0.282652 ± 16 (2SD, n = 4), respectively. The results are in good agreement with the accepted error of recommended values. All the Lu-Hf isotopic compositions are presented in the supplementary material (Supplementary data Tables S3 and S4) and a summary of the results are shown in Table 1.

We used the ^{176}Lu decay constant of λ = 1.867 10^{-11} yr^{-1} (Scherer et al., 2001; Söderlund et al., 2004), and parameters of the chondritic uniform reservoir (CHUR) ^{176}Lu/^{177}Hf = 0.0336 and ^{176}Hf/^{177}Hf 0.282785, values as suggested by Bouvier et al. (2008), for the calculation of initial ^{176}Hf/^{177}Hf ratios and $\varepsilon_{Hf}(t)$ values. Depleted Mantle (DM) values were calculated using a DM model considering linear regression from the present-day depleted mantle, as suggested by Blichert-Toft and Puchtel (2010), i.e., ^{176}-Lu/^{177}Hf = 0.03933 and ^{176}Hf/^{177}Hf = 0.283294. An average crustal ^{176}Lu/^{177}Hf ratio of 0.0113 was used for model age calculation (Taylor and McLennan,1995; Wedepohl, 1995).

5. Results

5.1. Zircon textures

Fifteen samples were collected for U–Pb analysis by LA-ICP-MS. All samples yielded a large number of zircon grains, but only a fraction (20%–50%) were considered appropriate for U-Pb dating. As demonstrated by Machado et al. (1992), Machado and Carneiro (1992), Noce et al. (1998), Lana et al. (2013), and Romano et al. (2013), zircons from the crystalline rocks of the SFC are largely altered and rich in mineral inclusions and fractures. Here we observed that the CA did not remove all the metamict discordant grains, but it substantially reduced the large volume of zircons affected by Pb-loss. We also observed that the chemically abraded zircons yielded the best CL images, making it easier to observe complex patterns of zircon growth, in addition to the presence/absence of xenocrystic cores, inclusions of other minerals, degree of fracturing, and metamictization.

Overall, the grain populations from different samples show similar internal structures, with multiple stages of zircon growth and alteration. Despite the textural complexity, we managed to recognize seven main groups of textures, which are essentially present in nearly all the samples (Fig. 4A). These include lobate domains (Fig. 4A, i), recrystallization fronts (Fig. 4A, ii), patchy and ghost textures (Fig. 4A, iii, iv) as well as spongy, metamict, and soccer ball zircons (Fig. 4A, v, vi, vii). In addition, we observed that spongy textured zircons are rich in metamict domains with fractures that served as pathways for fluid circulation, leaching radiogenic Pb and enriching the zircon in Pb_c. These domains are completely heterogeneous, structureless, and porous. Some grains show longitudinal streaks filled by new zircon growth (Fig. 4A). Finally, a small population of zoned zircons does not show any signs of resorption and/or recrystallization domains (B), indicating a magmatic origin.

5.2. U-Pb age dating

The U-Pb data was acquired in five daily sessions, where 15 samples collected all across the BHC were analyzed. A summary of the U-Pb ages for samples is presented in Table 1 (Supplementary data Tables S1 for details).

Sample BH-01 (UTM: 606777/7822490) represents a stromatic gneiss in the north of the complex (Fig. 1). The rock is characterized by the alternation of mm to cm-scale leucosomes (quartz + feldspar) and melanosomes (biotite + amphibole) bands and is intruded by leucogranitic sheets. The layers are oriented parallel to the main foliation. Locally, the layers and sheets are folded forming tight folds. Pegmatitic dikes also intrude the gneiss, cross-cutting the foliation. The zircon grains from the main stromatic gneiss preserve euhedral to sub euhedral prismatic shapes, with slightly round terminations, ranging in size from 100 μm to 300 μm long. They are generally white milky to brown and opaque to semi-translucent. The majority of the milky white grains are largely metamict and yielded unreliable U–Pb data (Machado et al.,

Table 1
Summary of the U-Pb and Lu-Hf data for samples of the Belo Horizonte Complex.

Sample	Studied rock	Location (UTM)	U-Pb age (Ma) 2σ	Interpreted age	ε_{Hf}	Hf model age	Magmatic event
BH-01	stromatic gneiss	606777/ 7822490	2814 ± 7 (MSWD = 2.1) *n* = 45	Crystallization	/	/	RVII
BH-02B	leucogranite	605190/ 7825093	2804 ± 3 (MSWD = 2.1) *n* = 75	Crystallization	(−4.9 to −2.0) *n* = 22	3.47–3.32 Ga	RVII
BH-02C	stromatic gneiss	605190/ 7825093	2864 ± 8 (MSWD = 1.06) *n* = 36	Crystallization	(−1.8 to −6.2) *n* = 9	3.35–3.58 Ga	RVI
BH-03	stromatic gneiss	565357/ 7841317	2856 ± 62 (MSWD = 4.3) *n* = 6 2716 ± 12 (MSWD = 1.4) *n* = 30 2619 ± 15 (MSWD = 1.9) *n* = 16	Protolith crystallization Migmatization Metamorphic	(−2.1) *n* = 1 (−3.3 to −1.7) *n* = 2 (−8.3 to −1.7) *n* = 3	3.25 Ga 3.30–3.22 Ga 3.50–3.24 Ga	RVI Mamona Mamona
BH-04	gneiss	606624/ 7800240	2706 ± 10 (MSWD = 0.40) *n* = 20	Crystallization	(−6.5 to −3.2) *n* = 16	3.46–3.28 Ga	Mamona
BH-05	stromatic gneiss	615986/ 7805284	2828 ± 33 ($^{207}Pb/^{206}Pb$) *n* = 1 2660 ± 12 (MSWD = 0.78) *n* = 17	Inherited Migmatization	(−0.7) *n* = 1 (−6.7 to −4.5) *n* = 10	3.26 Ga 3.44–3.34 Ga	RVII Mamona
BH-06	foliated granite	629157/ 7809112	2709 ± 6 (MSWD = 0.52) *n* = 21	Crystallization	(−3.7 to −1.9) *n* = 21	3.33–3.23 Ga	Mamona
BH-07A	stromatic gneiss	583025/ 7811506	2765 ± 14 (MSWD = 1.4) *n* = 23	Metamorphic	(−2.8 to −0.7) *n* = 4	3.30–3.21 Ga	Mamona
BH-07B	foliated granite	583025/ 7811506	2735 ± 15 (MSWD = 1.8) *n* = 22	Crystallization	(−0.5) *n* = 1	3.19 Ga	Mamona
BH-08A	stromatic gneiss	599430/ 7793023	2661 ± 11 (MSWD = 0.88) *n* = 19	Metamorphic	(−5.1 to −2.9) *n* = 5	3.37–3.26 Ga	Mamona
BH-08B	leucogranite	599430/ 7793023	2685 ± 19 Ma (MSWD = 3.1) *n* = 17	Crystallization	(−5.8) *n* = 1	3.43 Ga	Mamona
BH-09	migmatized	588087/ 7792313	2858 ± 59 ($^{207}Pb/^{206}Pb$) *n* = 1 2727 ± 13 (MSWD = 0.63) *n* = 23	Protolith crystallization Metamorphic	(−3.3 to −3.1) *n* = 3	3.31–3.30 Ga	RVII Mamona
BH-10	stromatic gneiss	575734/ 7813194	2758 ± 41 2682 ± 12 (MSWD = 2.3) *n* = 17	Protolith crystallization Metamorphic	(−5.0) *n* = 1 (−4.8) *n* = 1	3.44 Ga 3.36 Ga	Mamona
BH-12A	foliated K-granite	57798/ 7832145	2823 ± 35 ($^{207}Pb/^{206}Pb$) *n* = 1 2734 ± 12 (MSWD = 0.99) *n* = 22	Inhereted Crystallization	(0.6) *n* = 1 (−6.1 to 0.1) *n* = 6	3.18 Ga 3.50–3.16 Ga	RVII Mamona
BH-12B	foliated biotite-granite	577798/ 7832145	2830 ± 19 (MSWD = 0.3) *n* = 4 2680 ± 17 (MSWD = 1.8) *n* = 24	Inhereted Crystallization	(−4.9 to −2.5) *n* = 3 (−7.3 to −1.3) *n* = 5	3.50–3.28 Ga 3.47–3.28 Ga	RVII Mamona

1992; Machado and Carneiro, 1992; Lana et al., 2013; Romano et al., 2013). CL images from a subset of partly translucent brown zircons show broad zones of intense alteration and radiation damage. These zircons are dark and structureless, and some grains preserve cores with oscillatory zoning (Fig. 5). Fifty-one U-Pb analyses were performed on oscillatory zoning of 45 grains, yielding mostly discordant results. Forty-four points, plot along a regression line with an upper intercept at 2814 ± 7 Ma and lower intercept at 436 ± 34 Ma (2σ; MSWD = 2.1; Fig. 6A). Based on available textural information of the zircons we suggest that the upper intercept date is the best approximation of the crystallization age of the sample. The lower intercept is interpreted as Pb-loss in the Neoproterozoic Brasiliano event. Two spots on cores revealed the presence of >2940 Ma inherited zircons (2σ; MSWD = 1.8; Fig. 6A), but the points were significantly discordant. Another four spots on metamorphic rims gave a very imprecise intercept date of ca. 2780 ± 30 Ma, which is likely to be a metamorphic overgrowth age, but the points were too discordant to make further interpretations.

Samples BH-02B and BH-02C (UTM: 605190/7825093) were collected in the northern portion of the complex (Fig. 1). Sample BH-02C represents a stromatic gneiss characterized by the alternation of mm- to cm-scale leucocratic and mesocratic bands. BH-02B is a 0.2 m thick leucogranitic vein intruded into the stromatic gneisses BH-02C. Sample BH-02B contains fragments of zircon prisms that range in size from 100 μm to 300 μm and are subhedral to euhedral, slightly round, partly translucent to opaque, and milky white to brown. The milky white grains indicate some degree of metamictization. CL images exposed dark and structureless zircons. A subset of zircons shows patchy or broad zoning and convolute or oscillatory zoning (Fig. 5). Rare inclusions and fractured grains were also observed. Seventy-seven spots on 62 zircons were analyzed, but most of the U–Pb isotopic data are discordant, suggesting Pb loss at some stage of the evolution of these rocks. Seventy-five points located on oscillatory zoning of the grains define a regression line that intercepts the concordia at 2804 ± 3 Ma and 556 ± 19 Ma (2σ; MSWD = 2.1; Fig. 6B). The oscillatory zoning is typical of crystallization from a melt phase, and we interpret the upper intercept as the crystallization age of the sample. The lower intercept marks a Pb-loss event in the Neoproterozoic. Five spots located on structureless metamorphic rims of these grains yield a regression that intercepts the concordia at 2750 ± 10 Ma and 692 ± 54 Ma (2σ; MSWD = 0.92; Fig. 6B).

The zircon crystals and fragments from the Sample BH-02C, ranging in size from 50 μm to 300 μm, are euhedral to subhedral, vary from prismatic to slightly rounded in shape, are opaque to semi-translucent, reddish in color, and length/width ratios vary from 1:1 to 4:1. CL images reveal a weak intensity, oscillatory zoning, which is the most common internal structure; followed by patchy or broad zoning, and rarely convoluted zoning (Fig. 5). Some grains have a dark core surrounded by a lighter rim. Inclusions, fractured grains and local resorption and/or recrystallization features were also observed. A total of forty-two analyses on 29 zoned zircon grains yielded discordant U-Pb analyses. Thirty-six spots

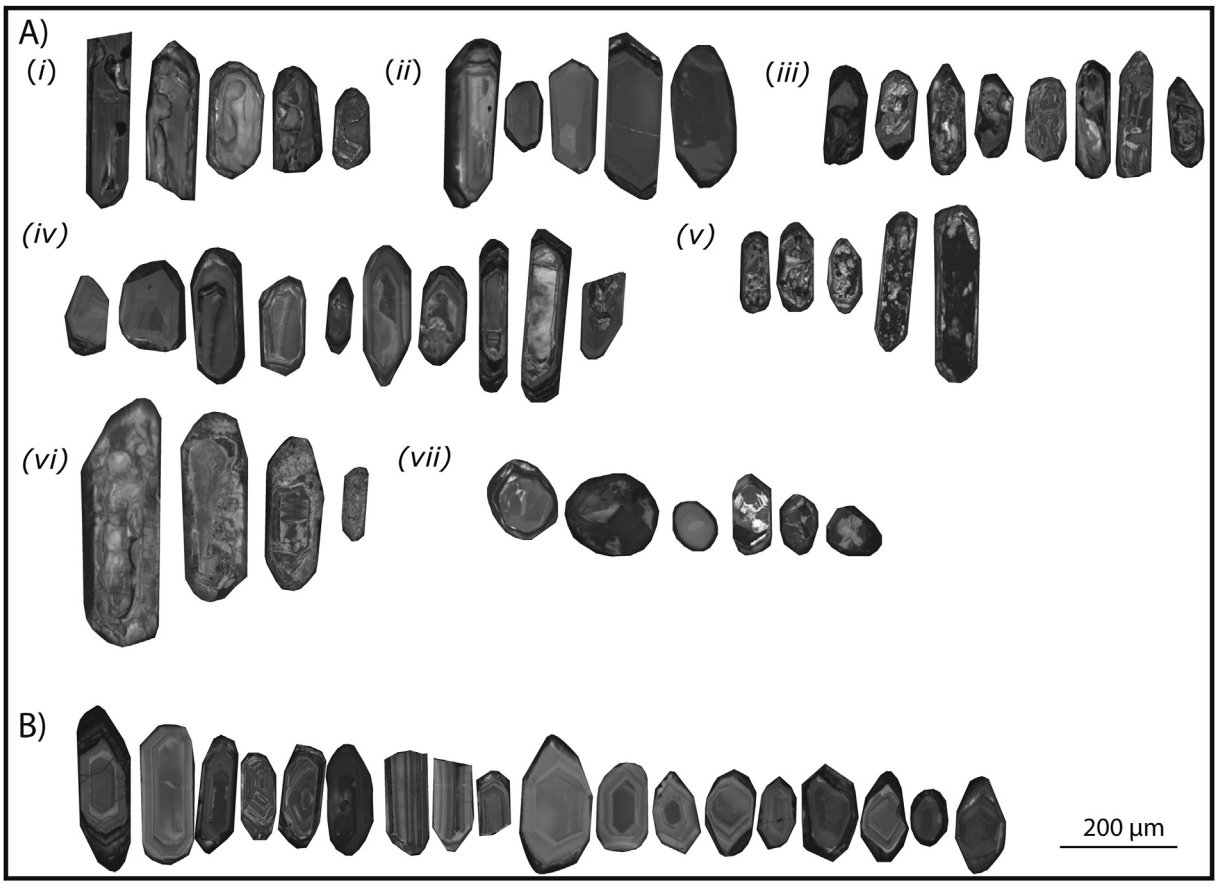

Fig. 4. (A) Examples of zircon textures identified in the Belo Horizonte Complex after the chemical abrasion. The zircon textures are classified as: (i) Lobate domains that truncate the original zoning. These domains replace the outer oscillatory zoning with irregular structureless domains, leaving the core partly preserved. (ii) Recrystallization fronts in which the grains show a progressive or a total replacement of the internal concentric zoning with featureless grey zones. In some cases, the grains may show a faint zoning or show structureless cores with thin metamorphic rims. (iii) Chaotic/patchy texture characterized by amoeboid patches with highly irregular patterns of recrystallization zones, either during a late magmatic stage or during subsequent metamorphism (Corfu and Ayres 1984). (iv) Ghost texture occurs in grains that preserve relics of the primary texture inside domains of recrystallization. Hoskin and Black (2000) suggest that this recrystallization may occur in solid-state. (v) Metamict texture is characterized by the complete destruction of an internal structure resulting in amorphous domains, as a result of secondary processes like recrystallization during interaction with a fluid phase (Geisler et al., 2007). (vi) Spongy texture shows a replacement of internal texture by cavities or porous domains, suggesting a metamorphic process like dissolution recrystallization (Xia et al., 2009). (vii) Soccer ball is external multifaceted shape, which commonly occurs in high-T process and display sector zoning and/or unzoned domains that crystallized in high-grade rocks during a metamorphic event (Corfu et al., 2003; Claesson et al., 2016). (B) Examples of well-preserved igneous zircons with well-developed oscillatory zoning, and no signs of resorption and/or recrystallization domains.

plot along a regression line with upper and lower intercept ages of 2864 ± 8 Ma and 552 ± 15 Ma (2σ; MSWD = 1.06; Fig. 6C). These zircons show clear igneous oscillatory zoning. Based on the field observations and CL textures, we interpret the upper intercept date as the crystallization age. The lower intercept relates to a Pb-loss event in the Neoproterozoic. Three cores revealed the presence of inherited older zircon, but these were too discordant (Fig. 6C). Three other spots on structureless rim overgrowths of three grains gave intercepts of 2665 ± 35 Ma and 508 ± 84 Ma (2σ; MSWD = 1.12; Fig. 6C). The upper intercept is interpreted as a metamorphic age and the lower intercept marks a Pb-loss event in the Neoproterozoic.

Sample BH-03 (UTM: 565357/7841317) is a stromatic gneiss collected from the northwestern portion of the complex (Fig. 1). The fine-grained migmatitic gneiss is marked by foliation-parallel leucogranite dikes, and both rock types are crosscut by late-stage pegmatitic dikes. Locally, a weakly-deformed granitoid (known as Pequi batholith – 2750 ± 13 Ma; Romano et al., 2013) is in intrusive contact with the gneiss. The sample includes fragments and zircon grains that are euhedral to subhedral prisms with rounded terminations varying from 100 to 300 μm in length, and partially translucent to brown in color. Most of the zircon cores display a complicated internal texture with local recrystallization and "sector" zoning (disruption of concentric oscillatory zoning), but no oscillatory zoning (Fig. 5), suggesting an isotopic disturbance. The data is very complex, as expected based on the migmatized nature of the sample. Six discordant spots corresponding to magmatic zircon cores gave a very poorly defined regression line with an upper intercept at ca. 2856 ± 62 Ma (MSWD = 4.3; Fig. 6D). The upper intercept is our best estimate of the magmatic crystallization age. A number of spot analyses (n = 30) on sector zoned, metamorphic zircons yield highly sub-concordant U-Pb ratios, with an upper intercept age of 2716 ± 12 Ma and lower intercept of 512 ± 10 Ma (2σ; MSWD = 1.4; Fig. 6D). Based on available textural information under CL we suggest that the upper intercept at 2716 ± 12 Ma is the best approximation for the age of partial melting, probably with the interaction between the emplacement of Pequi batholith or as a late-magmatic fluid. A third age is defined by a number of spots (n = 16) on the rims of small euhedral grains that gave an upper intercept age of 2619 ± 15 Ma and a lower intercept of 576 ± 31 Ma (2σ; MSWD = 1.9; Fig. 6D). The upper intercept age overlaps with the ages of several granitic bodies in the region

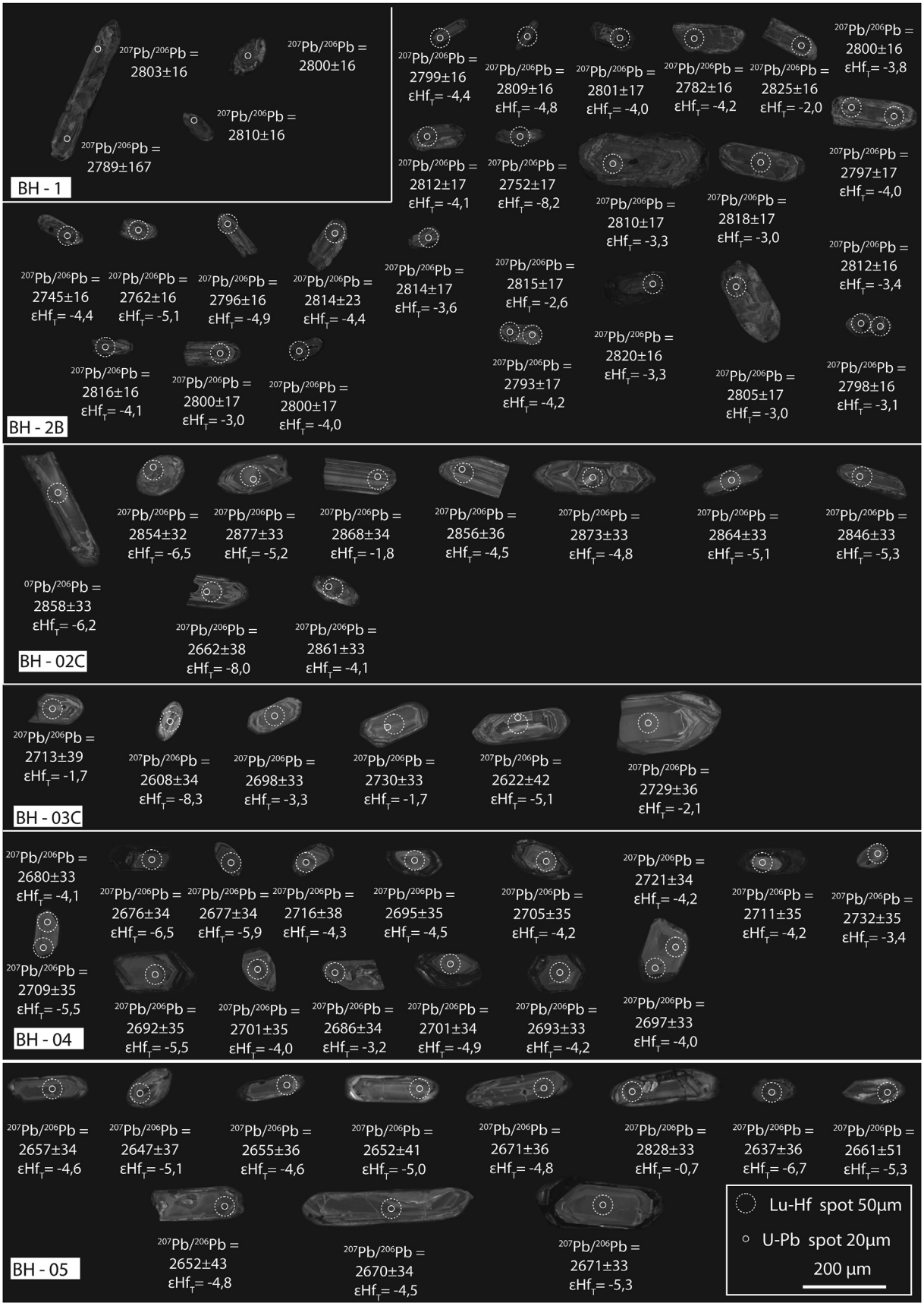

Fig. 5. Cathodoluminescence images of selected zircon grains that are concordant or near concordant. The circles indicate the laser spots position where the $^{207}Pb/^{206}Pb$ (spot size ~20 µm) ages, and dashed circles for Lu-Hf ($\varepsilon_{Hf}(t)$; spot size ~50 µm) were obtained. The scale is the same for all samples.

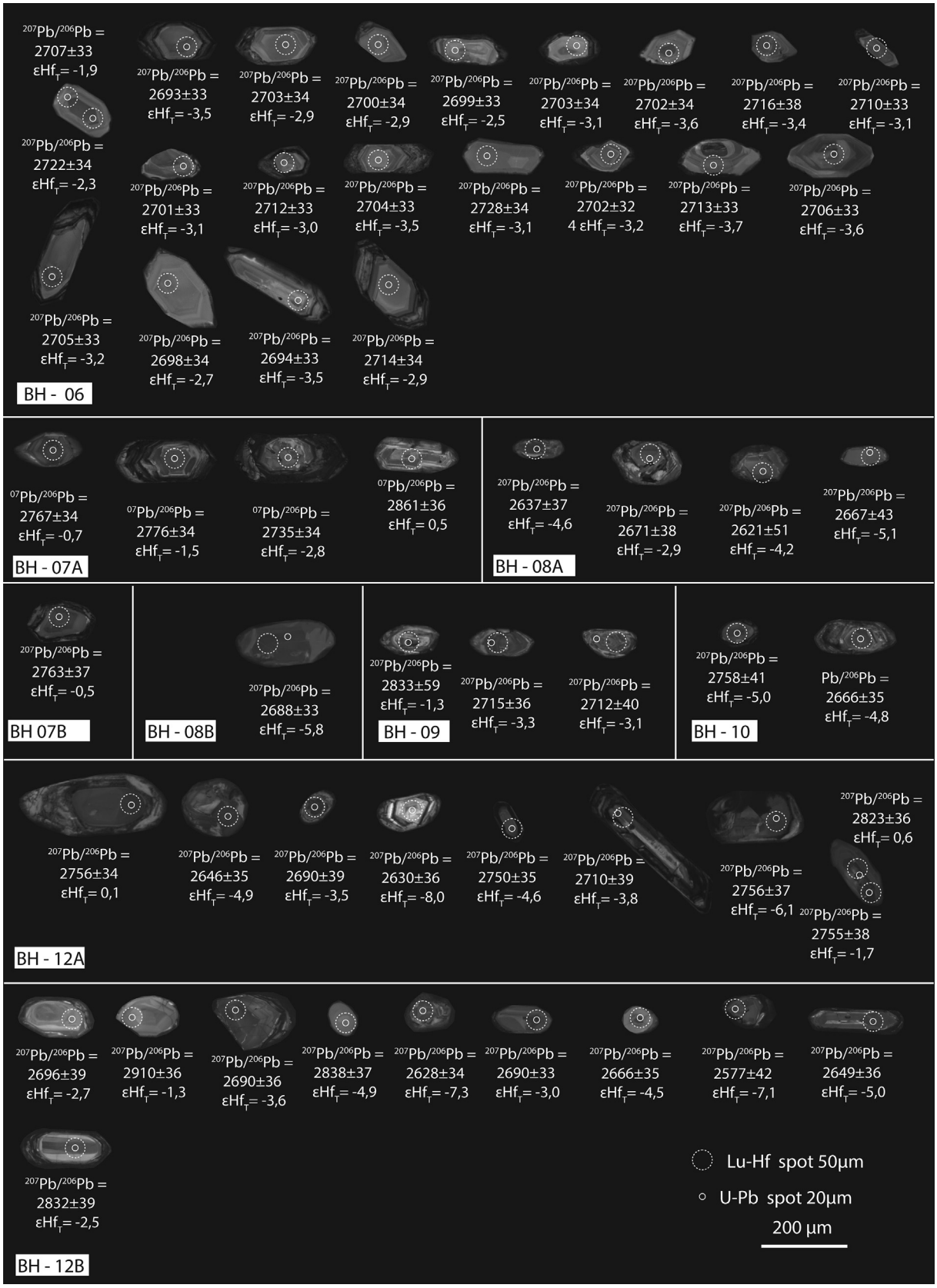

Fig. 5 (*continued*)

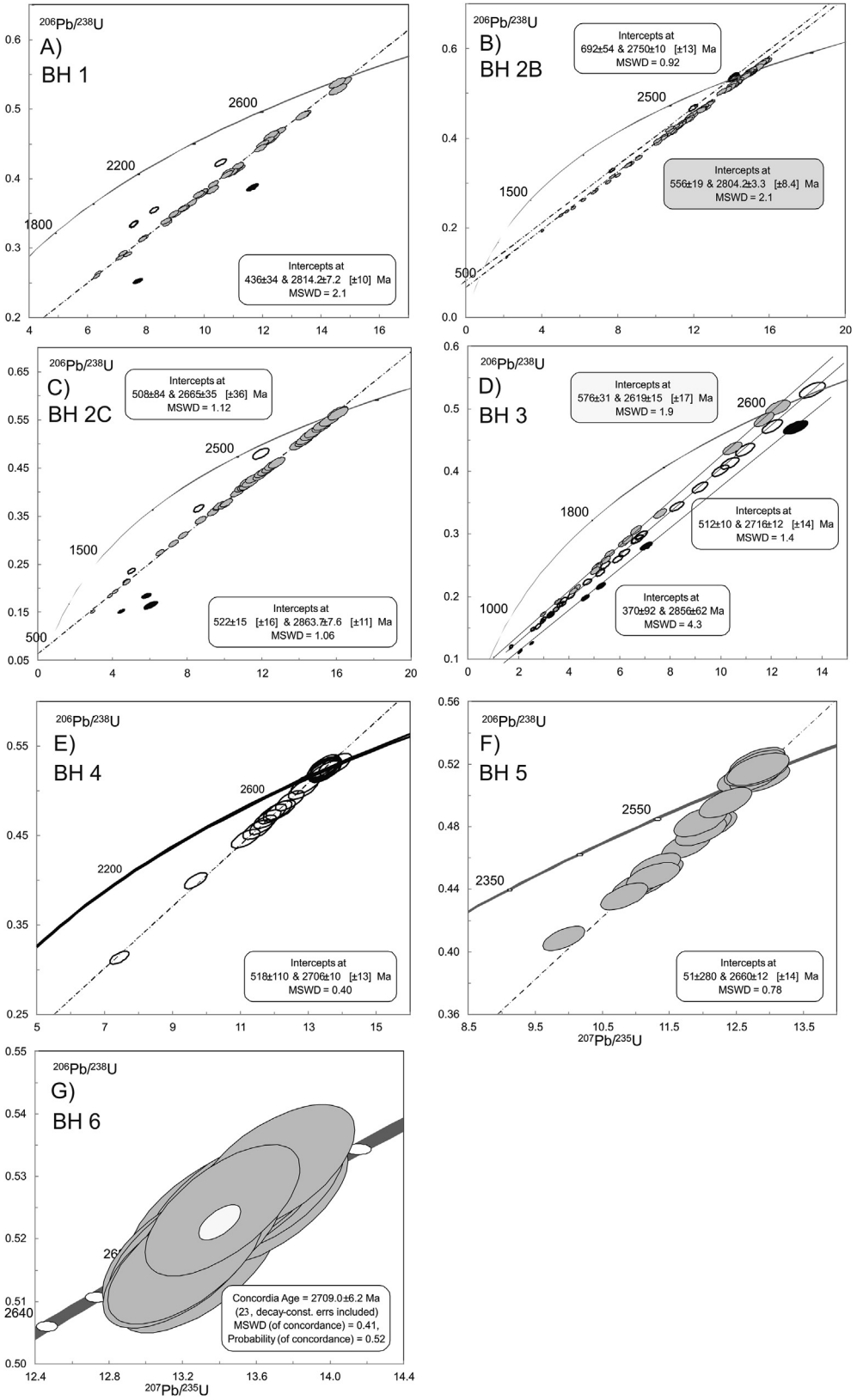

Fig. 6. U-Pb Concordia diagrams of LA-ICP-MS analyses from migmatites and leucogranites from the Belo Horizonte Complex. See Fig. 1 for sample localities.

(e.g., Romano et al., 2013) and probably reflects the age of the local injection of either mm-scale felsic bands or pegmatitic dikes, or a metamorphic event.

Sample BH-04 (UTM: 606624/7800240) is a fine-grained, weakly migmatized gneiss collected from an inactive quarry, inside the city of Belo Horizonte (Fig. 1). This rock is characterized by the alternation of mm to cm-scale leucocratic and mesocratic bands and by pegmatitic dikes, which crosscut or occur parallel to the foliation. The gneiss contains zircon grains that are brown in color, subhedral to euhedral, elongated to short prismatic, ranging in size from 100 μm to 200 μm and transparent to partially-transparent. The most common feature of the grains in CL is a core-rim structure. The cores reveal sector and faint and broad zoning. Some grains show bright cores surrounded by dark structureless rims (Fig. 5). A total of 20 core analyses, gave a Pb-loss regression line that intercepts the concordia at 518 ± 110 Ma and 2706 ± 10 Ma (2σ; MSWD = 0.4; Fig. 6E). We interpret the upper intercept as the crystallization age. The lower intercept is interpreted as a Pb-loss event in the Neoproterozoic.

Sample BH-05 (UTM: 615986/7805284) is a migmatized gneiss collected at a quarry in the central portion of the complex (Fig. 1). It exhibits stromatic, nebulitic, and phlebitic textures. The gneiss hosts amphibolite layers and non-foliated medium-grained leucogranite sheets with cm-scaled crystals of K-feldspar. The gneiss banding is characterized by the alternation between plagioclase and quartz-rich layers and amphibole and biotite-rich layers. Sample BH-05 is representative of the gneiss, in which leucosomes and melanosomes are mixed. Zircons from this sample range in size from 50 μm to 300 μm, and are transparent to partially-transparent and brown in color. Zircon grains are mostly prismatic and elongated, with a subset of zircons displaying short prismatic with round terminations. The grains contain inclusions of apatite and Fe-oxides and inherited cores. Patchy zoning is the most common textural type in zircon cores, as well as weakly oscillatory zoning (Fig. 5). Fracturing and alteration pathways and metamict zones indicate a late alteration (Corfu et al., 2003). Some zircon grains display core/rim structures. The rims were usually dark, and structureless, and too narrow to be analyzed. Seventeen of the most concordant to sub concordant points are aligned along a regression line with an upper intercept age of 2660 ± 12 Ma and a lower intercept at 51 ± 280 Ma (2σ; MSWD = 0.78; Fig. 6F). Based on the textural information we interpret the upper intercept to be the best approximation of the age of leucosome formation in the migmatitic orthogneiss. One spot on a core gave a concordant point with a $^{207}Pb/^{206}Pb$ age of 2828 ± 33 Ma. We interpreted date of 2828 ± 33 Ma to be an inherited age.

Samples BH-06 (UTM: 629157/7809112) is a medium to coarse-grained and slightly foliated yellow granitoid (known as the Córrego do Brumado granitoid) intruded into foliated TTG gneiss in the northeast of the complex (Fig. 1). Zircon crystals from this sample were euhedral to sub-euhedral, prismatic to elongated, slightly round, varying from 100 μm to 200 μm in length and brown in color. Most of the zircon grains in CL images display core/rim structures with bright cores surrounded by dark rims. Oscillatory zoning is the most common textural type in zircon cores, followed by broad zoning. The rims are structureless or present oscillatory zoning (Fig. 5). A total of 24 analyses on the cores were performed on 23 grains, and most of the U–Pb isotopic data are concordant. These grains form a tight population with a concordia age of 2709 ± 6 Ma (2σ; MSWD = 0.41; Fig. 6G), which is interpreted as the crystallization age. The metamorphic rims gave no reliable U-Pb results.

Samples BH-07A and BH-07B (UTM: 583025/7811506) were both collected from the central portion of the complex (Fig. 1). A migmatitic gneiss represents the main lithology in the outcrop and is similar to the banded gneisses sampled previously, but strongly migmatized. The rock hosts numerous mafic amphibolite enclaves. The amphibolite crops out as blocks, boudins, and lenses. Several leucogranitic and pegmatitic veins crosscut both the gneiss and the amphibolite. Sample BH-07A represents a migmatitic gneiss and sample BH-07B is from an intrusive granite. Sample BH-07A contains zircon grains ranging in size from 100 μm to 200 μm, elongated to prismatic, translucent to partly-translucent, and brown in color. Under CL, the grains are characterized by clear core-rim relationships. Most of the zircon cores reveal a complex internal texture, oscillatory and broad zoning superimposed by patchy, convolute, and sector textures, whereas the rims are structureless or weakly zoned (Fig. 5). The majority of the grains show local resorption and/or recrystallization features. Twenty-three analyses were conducted on the core and rims and resulted in twelve concordant to sub-concordant points that define a Pb-loss regression with a lower intercept of 479 ± 16 Ma and an upper intercept of 2765 ± 14 Ma (2σ; MSWD = 1.4; Fig. 7A). We suggest that the upper intercept date reflects a metamorphic age. The lower intercept is interpreted as Pb-loss during the Neoproterozoic Brasiliano event. The zircon cores gave very discordant points; five of them are inherited cores, which seem to indicate that the crystallization age of the protolith is ca. 2900 Ma. Zircons from sample BH-07B were highly metamict and the least altered zircon type consists of subhedral to euhedral crystals, prismatic to elongated, opaque to partially translucent, brown in color, and reaching 200 μm in length. Metamict domains are completely structureless and porous. Many of the zircon grains have broad oscillatory zones truncated by patchy and convolute zones that are grey in CL, with less grey and structureless rims (Fig. 5). A total of 22 analyses on the core and rims yielded highly discordant U-Pb ratios, with an upper intercept age of 2735 ± 15 Ma and a lower intercept of 518 ± 33 Ma (2σ; MSWD = 1.8; Fig. 7B). The upper intercept date is interpreted as the crystallization age of the granite. The lower intercept is interpreted as a result of Pb-loss in the Neoproterozoic Brasiliano event. Six other spots on cores seem to indicate inheritance but were too discordant to give meaningful ages.

Samples BH-08A and BH-08B (UTM: 599430/7793023) were collected from an inactive quarry near Contagem (Fig. 1). Sample BH-08A represents a stromatic gneiss characterized by the alternation of mm-scale leucocratic and mesocratic bands. BH-08B is a leucosome portion of a nebulitic domain. Mafic xenoliths are also common and crop out as lenses and enclaves. Sample BH-08A contains brown zircon grains, varying in size from 100 μm to 200 μm, subhedral to euhedral, partly translucent to opaque. The majority of the zircon crystals have an unzoned and homogeneous core, surrounded by a structureless rim. The core-rim features exhibit different brightness in CL images. A subset of grains shows homogeneous and grey outer domains that surrounds inner domains with fine oscillatory zoning (Fig. 5). Inherited cores are also present. Nineteen spots on the structureless, unzoned rims of these zircons define a Pb-loss line with an upper intercept age of 2661 ± 11 Ma and a lower intercept of 406 ± 22 Ma (2σ; MSWD = 0.88; Fig. 7C). Based on the CL textures we interpret the upper intercept to be a metamorphic age. The lower intercept marks a Pb-loss event in the Neoproterozoic. Four other spots on cores seem to align along a poorly defined regression with an upper intercept age of ca 2800 Ma, which is likely to represent an inherited age from the basement rocks. The zircon grains from sample BH-08B are prismatic to elongated with slightly rounded terminations, ranging in size from 100 μm to 200 μm, brown in color, euhedral to subeuhedral, and translucent to partly-translucent. In CL, the grains show a clear core-rim relationship. The cores reveal a complex internal texture, with relics of oscillatory zoning, and local recrystallization along longitudinal microfractures. In contrast the overgrowths are dark and structureless or weakly zoned (Fig. 5). A total of 20 analyses were performed

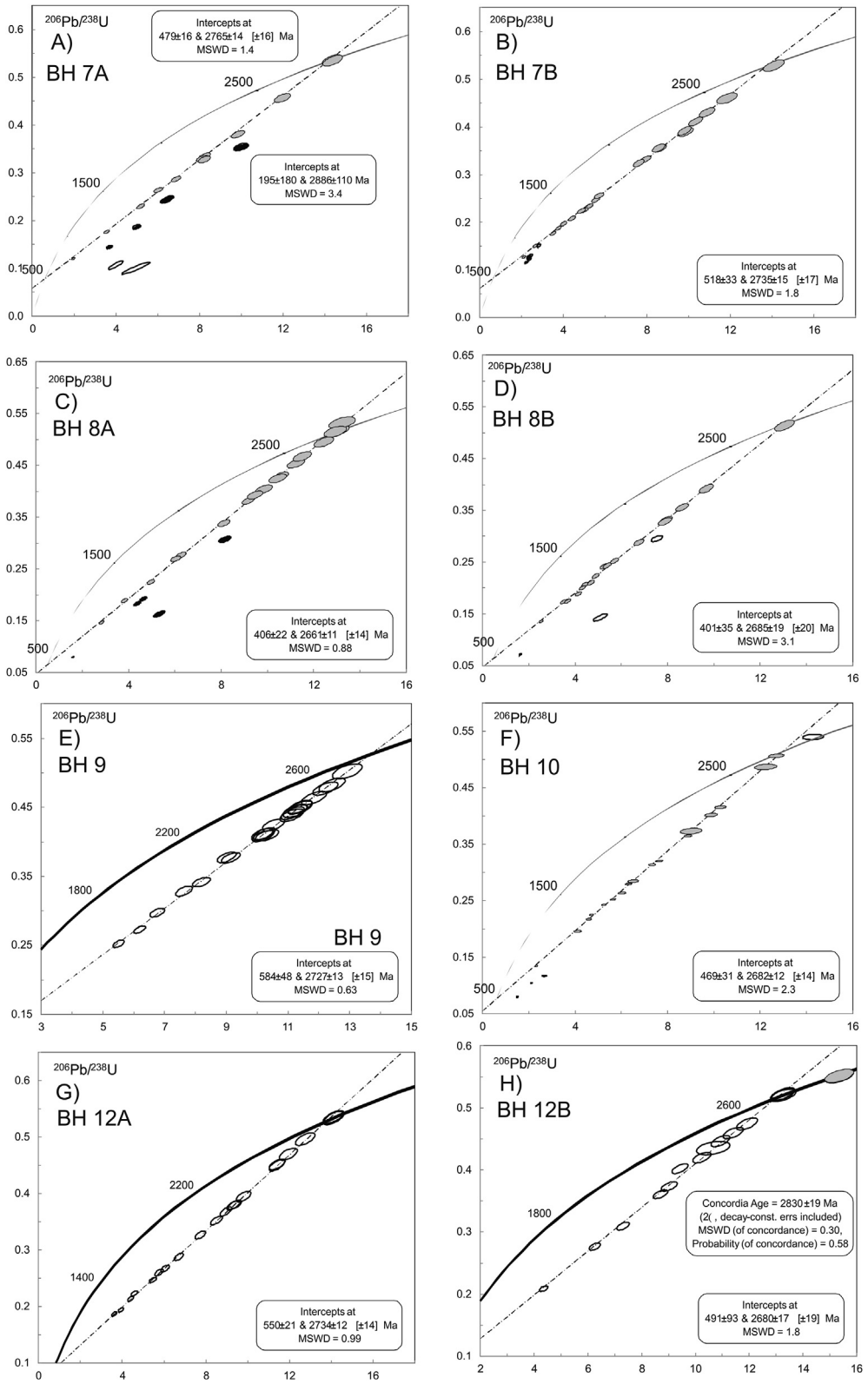

Fig. 7. U-Pb Concordia diagrams of LA-ICP-MS analyses from migmatites and leucogranites from the Belo Horizonte Complex. See Fig. 1 for sample localities.

on preserved oscillatory zoning of 20 grains. Seventeen spots plot along a regression line with an upper intercept age of 2685 ± 19 Ma and a lower intercept at 401 ± 35 Ma (2σ; MSWD = 3.1; Fig. 7D). This upper intercept is within error of the age of sample BH-08A and is interpreted as the age of crystallization of the leucosome. The lower intercept is interpreted as a Pb-loss in the Neoproterozoic Brasiliano event.

Sample BH-09 (UTM: 588087/7792313) represents a strongly migmatized orthogneisses occurring in the south of the complex (Fig. 1). The rock is characterized by the alternation of mm- to

cm-scale leucosome (quartz + feldspar) and melanosome (biotite + amphibole) bands, and is intruded by numerous leucogranitic dikes and pinkish pegmatitic bodies. This sample, in which leucosomes and melanosomes are mixed, contains zircon grains that are sub-euhedral, short prismatic to slightly rounded, above 200 μm in length, and brown in color. The grains exhibit magmatic oscillatory zoning, with some chaotic internal structures (patchy and convolute zoning) in CL images (Fig. 5). Such textures are consistent with local recrystallization during medium to high temperature metamorphism (Corfu et al., 2003). Fracturing and inclusions are also common. Some grains show a bright structureless overgrowth surrounding the cores. Twenty-three analyses were determined in the core and rims from this sample, and eighteen sub-concordant to concordant grains plot along a Pb-loss discordia. A regression line through these analyses intercepts the concordia at 584 ± 48 Ma and 2727 ± 13 Ma (2σ; MSWD = 0.63; Fig. 7E). The upper intercept age of 2727 ± 13 Ma is the best approximation of the age of leucosome formation of this migmatitic orthogneiss. The lower intercept relates to a Pb-loss event in the Neoproterozoic. One analysis on the core of this sample gave a concordant age of ca. 2858 Ma, which was interpreted as an inherited age.

Sample BH-10 (UTM: 575734/7813194) represents a stromatic gneiss in the central sector of the complex (Fig. 1). The rock is characterized by the alternation of mm- to cm-scale leucosome (quartz + feldspar) and melanosome (biotite + amphibole) bands, and is intruded by leucogranitic sheets and pegmatitic bodies parallel to the foliation. Zircon grains are sub-euhedral crystals, short prismatic or bipyramidal, varying from 100 μm to 200 μm in length, translucent, and brown in color. In CL images, some grains reveal core/rim structures. Most of the zircon cores display complex internal textures. The cores exhibit weak oscillatory zoning interrupted by several resorption surfaces (Fig. 5). Truncation of patchy and broad textures are also common and indicates local recrystallization, which suggests a metamorphic event. Some grains show bright cores surrounded by dark structureless overgrowths. Twenty-two spots on the zircon overgrowths gave mostly discordant points, suggesting isotopic disturbance. Seventeen of these points define a regression line that intercepts the concordia at 2682 ± 12 Ma and 469 ± 31 Ma (2σ; MSWD = 2.3; Fig. 7F). The upper intercept age can be interpreted as the metamorphic age given that the spots were only on the structureless overgrowths. The lower intercept is interpreted as a Pb-loss in the Neoproterozoic Brasiliano event. One concordant analysis with a $^{207}Pb/^{206}Pb$ age of 2758 ± 17 Ma can be interpreted as a possible crystallization age for the igneous protolith. Three other spots were too discordant to give meaningful ages.

Samples BH-12A and BH-12B (UTM: 577798/7832145) are from the northwest part of the complex, a few kilometers from the contact with the Pequi batholith (Fig. 1). Sample BH-12A, which represents the main lithology in the outcrop, is a coarse-grained foliated granite, pink in color, which locally has a porphyritic appearance given by the occurrence of large microcline crystals of up to 3 cm. Sample BH-12B is from a fine-grained foliated biotite-bearing granite that intrudes the gneiss host rock. Zircons from this sample are prismatic to stubby, subhedral to euhedral, reaching 300 μm in length, transparent to partly-transparent, and brown in color. Cathodoluminescence images display a great variety of internal textures with convolute and patchy zoning in the cores. Most of the grains show weak oscillatory zoning interrupted by several resorption surfaces (Fig. 5). The elevated degree of fracturing and alteration pathways and metamict zones indicate late alteration (Corfu et al., 2003). Inherited cores were also observed. A subset of zircon grains shows a bright structure-less domains. Twenty-six spots on preserved oscillatory zoning of 25 grains were analyzed, and most of the U-Pb data were discordant. One single grain shows a concordant $^{207}Pb/^{206}Pb$ age of 2823 ± 36 Ma, and represents an inherited age. A regression line of twenty-two analyses yields an upper intercept date of 2734 ± 12 Ma and a lower intercept of 550 ± 21 Ma (2σ; MSWD = 0.99; Fig. 7G). The upper intercept is interpreted as the best approximation for the age of the crystallization of the sample. The lower intercept is interpreted as Pb-loss during the Neoproterozoic Brasiliano event. Sample BH-12B contains zircon grains that are subhedral to euhedral, short prismatic to stubby, ranging in size from 50 μm to 200 μm, and translucent to party-translucent. The most common feature of the crystals in CL is core-rim structures. The cores reveal oscillatory and broad zoning, truncated by patchy, sector and convolute textures (Fig. 5). Some grains show bright cores surrounded by dark structureless overgrowths. Xenocrystic cores were observed and display unzoned features or poor oscillatory zoning. Metamict domains are pervasive and defined by corroded edges, fracturing and dark structureless grains. The majority of the crystals display local resorption and/or recrystallization features. Twenty-four spots (analyzed on preserved oscillatory zoning of 24 grains) gave a regression line with an upper intercept age of 2680 ± 17 Ma and a lower intercept at 491 ± 93 Ma (2σ; MSWD = 1.8; Fig. 7H). The upper intercept age is considered the best approximation of the crystallization age of the sample. The lower intercept marks a Pb-loss event in the Neoproterozoic. Four other points obtained on cores (of which two were concordant) suggest an inherited age of ca. 2830 ± 19 Ma.

5.3. Lu-Hf isotopes

Lu-Hf isotopes were analyzed on the same zircon domain previously analyzed by U-Pb. The Lu-Hf spots were located only on those grains which were>95% concordant in the U-Pb system. The results for all individual zircon grains are shown in a plot of initial Hf ($\varepsilon_{Hf}(t)$) vs. U-Pb age (Fig. 8), and the results are listed in Supplementary data Tables S3. The Lu-Hf and U-Pb analyses in zircon are used here to distinguish the magma sources and partial melting events.

We obtained a total of 126 Hf isotopic determinations: 25 on sample BH-02B; 10 on sample BH-02C; 6 on sample BH-03; 16 on sample BH-04; 11 on sample BH-5; 21 on sample BH-6; 4 on sample BH-07A; 1 on sample BH-07B; 5 on sample BH-08A; 2 on sample BH-08B; 3 on sample BH-09; 2 on sample BH-10; 9 on sample BH-12A; 11 on sample BH-12B.

The Lu–Hf analyses on magmatic zircon cores (sample BH-02C) yielded heterogeneous $^{176}Hf/^{177}Hf_{(t)}$ ratios from 0.280764 to 0.280888. The $\varepsilon_{Hf}(t)$ values are negative, ranging from −1.8 to −8.0, with T_{DM} model ages of 3.35–3.53 Ga. One analysis of an inherited zircon (2910 Ma) from sample BH-12B gives a $^{176}Hf/^{177}Hf_{(t)}$ ratios of 0.280872, with $\varepsilon_{Hf}(t)$ value of −1.3 and T_{DM} model age of 3.36 Ga.

Lu–Hf analyses from sample BH-02B show $^{176}Hf/^{177}Hf_{(t)}$ ratios that vary from 0.280842 to 0.280910. The $\varepsilon_{Hf}(t)$ values are negative, range from −4.9 to −2.0, with T_{DM} model ages of 3.47–3.32 Ga. A younger cluster of three crystals yielded $^{176}Hf/^{177}Hf_{(t)}$ ratios that vary from 0.280783 to 0.280893, with $\varepsilon_{Hf}(t)$ values ranging from −8.2 to −4.4 and T_{DM} model ages ranging from 3.34 to 3.13 Ga. One inherited zircon from sample BH-05 with an age of 2828 Ma gives a $^{176}Hf/^{177}Hf_{(t)}$ of ratio 0.280945, corresponding to an $\varepsilon_{Hf}(t)$ value of −0.7 and T_{DM} model age of 3.26 Ga. Two inherited zircons from sample BH-12B with an age 2805 Ma gave $^{176}Hf/^{177}Hf_{(t)}$ ratios ranging of 0.280820 and 0.280892, and $\varepsilon_{Hf}(t)$ values vary between −4.9 and −2.5 (T_{DM} model ages of 3.23 Ga and 3.09 Ga). Finally, one inherited zircon from sample BH-12A with age 2817 Ma shows a higher $^{176}Hf/^{177}Hf_{(t)}$ ratio of 0.281007, with an $\varepsilon_{Hf}(t)$ positive value of +0.3 and a T_{DM} model age of 3.18 Ga.

The younger cluster (defined by magmatic zircons from BH-06, BH-07A, BH-07-B, BH-12A and BH-12B) shows $^{176}Hf/^{177}Hf_{(t)}$ ratios

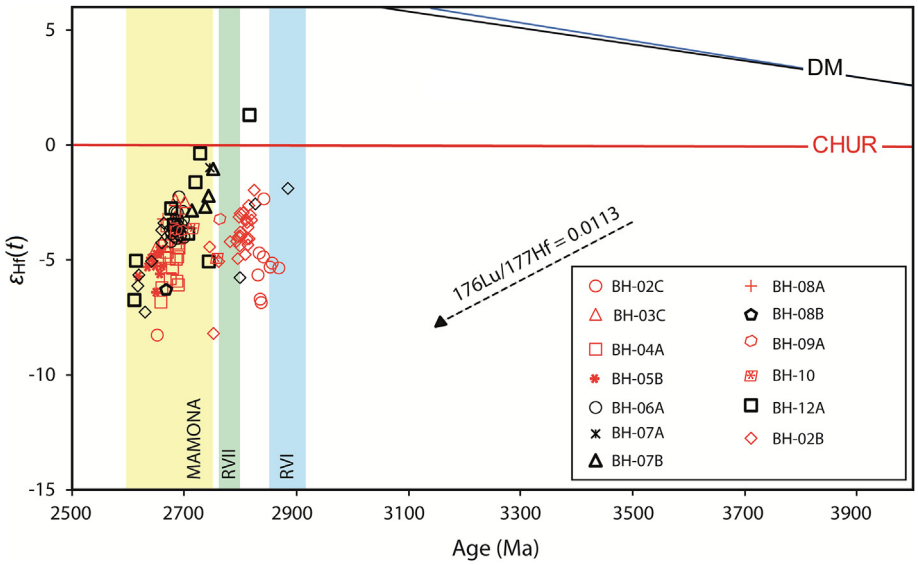

Fig. 8. $^{176}Hf/^{177}Hf_{(t)}$ versus apparent $^{207}Pb/^{206}Pb$ age diagrams for individual analyses with >95% concordance. Reference lines are: depleted mantle according to Griffin et al. (2000) ($^{176}Hf/^{177}Hf$ = 0.283250 and $^{176}Lu/^{177}Hf$ = 0.0384) and T_{DM} calculations using the $^{176}Lu/^{177}Hf$ and $^{176}Hf/^{177}Hf$ ratios of 0.03933 and 0.283294 (Blichert-Toft and Puchtel, 2010), CHUR constants ($^{176}Hf/^{177}Hf$ = 0.282785 and $^{176}Lu/^{177}Hf$ = 0.0336) of Bouvier et al. (2008). Red symbols are from migmatites and black symbols from granites or leucosomes. Vertical bars indicate Rio das Velhas I (RV I), Rio das Velhas II (RV II) and Mamona magmatic events.

ranging from 0.280876 to 0.281018, with $\varepsilon_{Hf}(t)$ values ranging from −7.3 to −0.4 and T_{DM} model ages ranging from 3.43 Ga to 3.14 Ga. In contrast to the magmatic zircons, metamorphic grains show a narrow $^{176}Hf/^{177}Hf_{(t)}$ ratio range of 0.280881 to 0.280993, with $\varepsilon_{Hf}(t)$ values varying from −6.4 to −2.4 and T_{DM} model ages ranging from 3.44 Ga to 3.21 Ga.

6. Discussion

6.1. Antiquity of the Archean crust in the Belo Horizonte Complex

Despite the extensive period of partial melting and migmatization recorded in the basement rocks of the BHC, our results show that some foliated gneisses and migmatites record crystallization and inherited ages, and that both overlap well with the main peaks of granitoid production in the southern part of the SFC (e.g., RVI, RVII and Mamona: Fig. 2). For example, the RVI event is represented by the emplacement of the 2863 ± 8 Ma, 2856 ± 62 Ma and 2858 ± 59 Ma gneisses in the northern and southern portion of the complex (Sample BH-02C, Sample BH-03 and Sample BH-09 respectively; Fig. 9). The oldest zircon core (that yielded the $^{207}Pb/^{206}Pb$ age of 2910 ± 36 Ma in sample BH-12B) is also interpreted as inherited from the RV I event. The second set of crystallization ages (are interpreted as part of the RV II event) and marked by the emplacement of granitoids and leucogranitic veins at ca. 2814–2804 Ma. Samples BH-01 and BH-02B best depict this group of rocks, and are found in the north of the BHC (Fig. 9).

In terms of crustal sources, the RVI and RVII rocks represent crustal reworking of older crustal material without substantial addition of juvenile magmas. Much of the $\varepsilon_{Hf}(t)$ values are negative, ranging from −6.2 to −1.8, with T_{DM} model ages of 3.35–3.58 Ga (Table 1). We note that despite the lack of older inherited zircon, T_{DM} model ages indicate reworking of even older crustal material that was extracted from mantle between 3.30 Ga and 3.40 Ga. The existence of Paleoarchean continental crust older than 3.2 Ga is also supported by the Sm-Nd model ages of the TTG gneiss (Teixeira et al., 1996), which also indicates the involvement of a crustal component in their origin (Lana et al., 2013; Farina et al., 2015; Albert et al., 2016).

The U-Pb age compilation for the southern SFC (Figs. 9 and 10) shows that all basement complexes forming the Archean crystalline crust record magmatic assemblages that crystallized roughly within identical cycles of the RVI and RVII event. This includes not only the TTG rocks, but also the low, medium and high potassium magmatic assemblages. Also, all the basement complexes such as the Bação, Bonfim and Belo Horizonte seem to record a long-lived period of high-grade metamorphism and partial melting from 2750 Ma to 2600 Ma (Fig. 10). Based on our U-Pb and Hf dataset we suggest that the BHC is part of a much larger crustal fragment that may have included all basement complexes exposed in the southern part of the SFC. The compiled ages in Figs. 9 and 10 show these complexes share a multi-stage evolution from 3000 Ma, which included magmatic and metamorphic processes associated with the RVI, RVII and Mamona events (e.g., Fig. 1). We propose that the RVI and RVII involved a combination of crustal reworking and minor additions of juvenile TTG magmas in a Paleoarchean crust (see also Albert et al., 2016). These events were accompanied by voluminous additions of mafic and ultramafic rocks represented by the basal units of the Rio das Velhas Supergroup and greenstone belt remnants across the southern part of the SFC.

6.2. Discrete episodes of partial melting

Partial melting of the Archean basement rocks and migration of potassium-rich melts may have played a significant role in the exchange of radioactive elements (and heat transfer) from the lower to the upper crust of the SFC (Lana et al., 2013; Romano et al., 2013). We observed that melting, melt drainage, and melt accumulation in plutons is a significant feature in the BHC, and is likely a feature in other basement complexes of the SFC (e.g., Lana et al., 2013). In terms of zircon textures, the most common feature indicative of partial melting are highly resorbed cores, surrounded by thin rim overgrowths (e.g., Fig. 5). The zircon cores show relics of oscillatory zoning partly or completely truncated by very pervasive recrystallized zones, which suggest recrystallization and/or resorption at medium to high metamorphism temperature (Corfu et al., 2003). Other zircons crystals are marked by

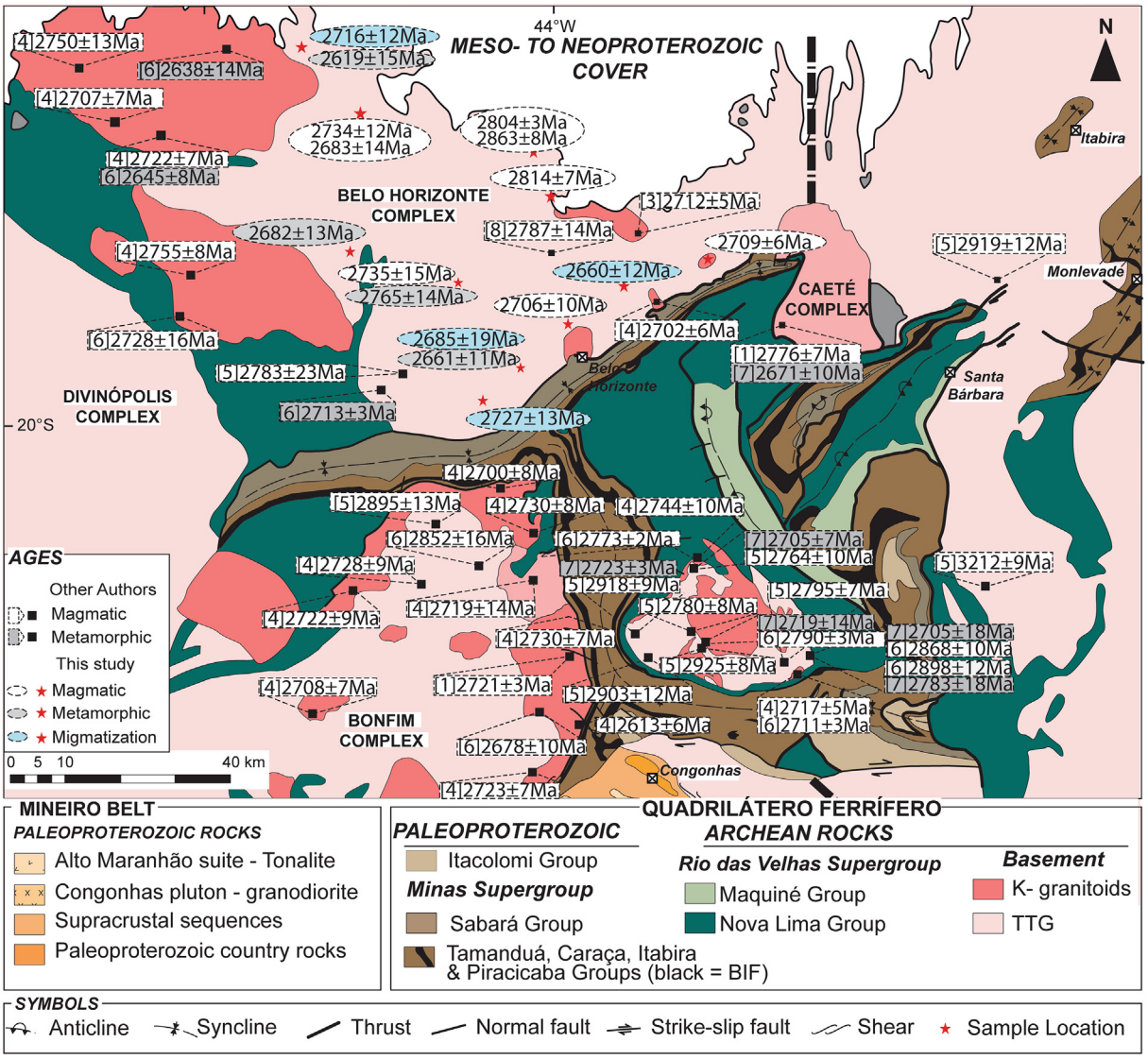

Fig. 9. Geological map of the southernmost São Francisco Craton showing the dates of zircon ages obtained in this study and previously published ages. Squares indicate the previously ages from other authors and stars from this study. Reference: [1] Machado et al. (1992); [2] Machado and Carneiro (1992); [3] Noce et al. (1998); [4] Romano et al. (2013); [5] Lana et al. (2013); [6] Farina et al. (2015); [7] Albert et al. (2016); and [8] Silva et al. (2012).

features such as (i) lobate fronts truncating the original zoning and replacing the primary zoning by a structureless rim; (ii) recrystallization with partial to complete replacement of internal concentric zoning; (iii) chaotic/patchy textures marked by amoeboid patches and highly irregular patterns of recrystallization zones; and (iv) ghost textures occurring in grains that preserve relics of primary textures inside domains of recrystallization (e.g., Figs. 4 and 5).

Careful observation of the individual zircon domains that U-Pb data was obtained from, allows us to define the timing of contemporaneous metamorphic resetting and crystallization of multiple melt batches of potassic rocks. Overall, the magma batches were likely produced during three main discrete anatectic periods (or stages) from 2750 Ma to 2600 Ma (Fig. 11). The first partial melting stage (Stage I) occurred at 2760 Ma to 2750 Ma and is best recorded by samples BH 07A and BH-10 with crystallization ages 2765 ± 14 Ma and 2758 ± 41 Ma. The ages overlap with the age of the youngest felsic volcanic units in the Rio das Velhas greenstone belt, the oldest pulse of potassic granitoid magmatism, and mafic intrusions in the Carmópolis de Minas Layered Suite (Romano, 1989; Campos and Carneiro, 2008; Goulart et al., 2013; Lana et al., 2013; Romano et al., 2013; Moreno et al., 2017; Fig. 10). Large batholiths emplaced in the western and northwestern areas of the complex, such as the Florestal and Pequi batholiths, yielded identical crystallization ages of 2755 ± 8 Ma and 2750 ± 13 Ma, respectively (Romano et al., 2013; Fig. 9). Another sample collected to the south of the Florestal batholith by Romano (1989) gave an upper intercept age of 2755 ± 14 Ma and an orthogneiss and a granodiorite exposed to the north of the Bação Complex crystallized at 2764 ± 10 Ma and 2744 ± 10 Ma, respectively (Lana et al., 2013; Romano et al., 2013). To the southwest of the BHC, ages of ca. 2750 Ma were obtained for granites and migmatitic gneisses by Campos and Carneiro (2008) and Oliveira (2004); and more recently Moreno et al. (2017) described an identical crystallization age of 2748 ± 5 Ma from a highly porphyritic biotite orthogneiss from the same area. Finally, a metamorphic age of 2749 ± 10 Ma, which reflects the crystallization of the foliation parallel leucogranite sheets in the Brumadinho banded trondhjemite was obtained by Lana et al. (2013) (Fig. 10).

The second stage (Stage II) of partial melting and leucosome crystallization ranges from 2735 Ma to 2700 Ma and is defined by samples BH-03, BH-04, BH-06, BH-07B, BH-09, and BH-12A.

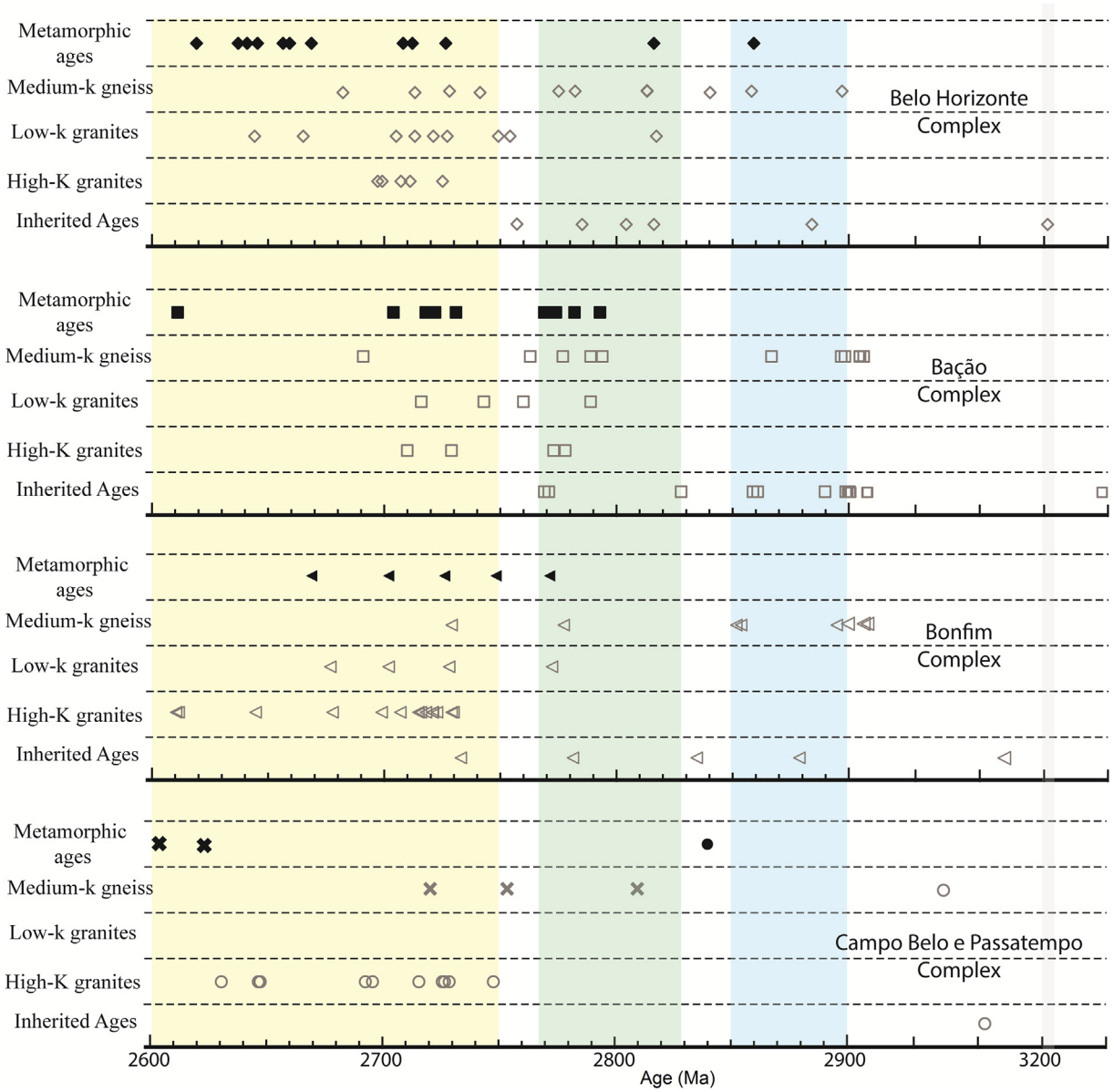

Fig. 10. Timeline showing U-Pb ages for the best-studied basement complexes in the southern SFC (e.g., Belo Horizonte, Bação, Bonfim, Campo Belo e Passatempo complexes). Black symbols are for metamorphic zircon ages and light grey from crystallization and inherited zircon ages. The vertical fields indicate the different magmatic events: Santa Bárbara (grey); Rio das Velhas I (blue); Rio das Velhas II (green); Mamona (yellow). Data are from Machado and Carneiro (1992); Chemale et al. (1993); Machado et al. (1992); Noce et al. (1998); Noce et al. (2005); Campos and Carneiro (2008); Goulart et al. (2013); Lana et al. (2013); Romano et al. (2013); Farina et al. (2015, 2016); Albert et al. (2016); Carvalho et al. (2017); Moreno et al. (2017); Simon et al., (2018).

These ages coincide with the second stage of potassic granitoid magmatism between 2730 Ma and 2700 Ma (Romano et al., 2013; Farina et al., 2016), including the Mamona, Souza Nochese, Piracema, General Carneiro, Santa Luzia and the youngest magmatic phase in the Florestal and Pequi granitoids, and their associated leucogranitic intrusions in the Bação and Bonfim complexes. Likewise, crystallization ages of 2729 ± 4 Ma, 2726 ± 4 Ma, 2727 ± 7 Ma, 2718 ± 13 Ma, and 2716 ± 6 Ma have been reported from the Campo Belo Complex (Moreno et al., 2017). Farina et al. (2015) dated an amphibolitic dike in the center of the Bonfim dome at 2719 ± 14 Ma, which corresponds very well in age with the crystallization of the oldest mafic dike in the northern SFC (2726 Ma; Oliveira et al., 2010). This period ends with the emplacement of localized granitoid intrusions in all basement complexes, including 2712 ± 5 Ma, 2700 ± 5 Ma and 2698 ± 5 Ma granitic phases in the BHC, a small 2708 ± 7 Ma granite intrusion in the Bonfim Complex, and minor leucogranite intrusions in the Pequi and Souza Nochese batholiths dated at 2707 ± 7 Ma and 2700 ± 8 Ma (Chemale et al., 1993; Noce et al., 1998; Romano et al., 2013). In the Campo Belo Complex, the waning stages of this period are marked by 2704 ± 4 Ma, 2696 ± 6 Ma and 2693 ± 16 Ma granitoids (Carvalho et al., 2017; Moreno et al., 2017) (Fig. 10).

The third stage (Stage III) is the most strongly expressed in the BHC. It ranges in age from 2680 Ma to 2614 Ma and is indicated by granitoid samples BH-03, BH-05, BH-08A, BH-08B, BH-10, and BH-12B that gave ages of 2619 ± 15 Ma, 2660 ± 12 Ma, 2661 ± 11 Ma, 2685 ± 19 Ma, 2682 ± 13 Ma, and 2683 ± 14 Ma respectively. Although Romano et al. (2013) showed that the main peak of granitic magmatism took place between 2750 Ma and 2700 Ma with small granitoid intrusions at 2612 Ma (Noce et al., 1998; Romano et al., 2013; Fig. 10), our dataset and the U-Pb ages documented for Campo Belo and São Tiago granitoids reveal prominent

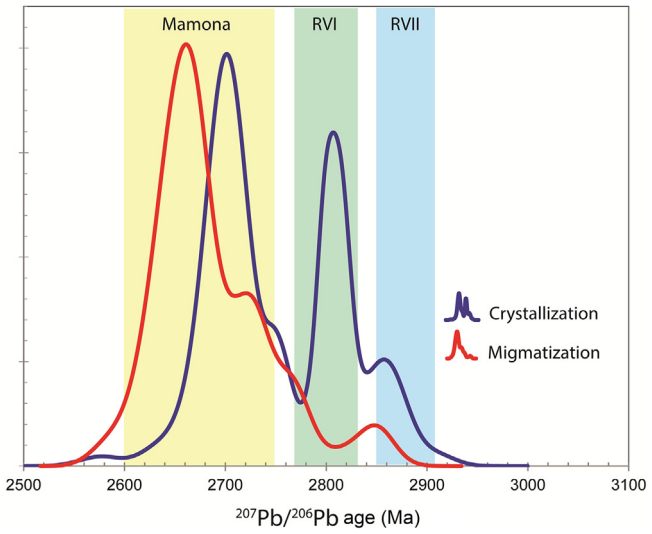

Fig. 11. Compilation of crystallization ages vs. metamorphic/migmatization ages for the crystalline rocks intruded in the basement rocks of the Belo Horizonte Complex.

magmatism taking place after 2700 Ma (Fig. 11), with the intrusion of leucogranitic dikes at 2680, 2650 and 2631 Ma (Moreno et al., 2017; Simon et al., 2018). Additionally, reworking under granulite facies metamorphism and migmatization were pointed out by Teixeira et al. (1998) at ca. 2661 ± 36 Ma (Rb-Sr isochron) in the Passa Tempo Complex. Work by Campos et al. (2003) also identified the age of 2622 ± 18 Ma via U-Pb dating.

In summary, the U-Pb and Hf datasets for the melt phases indicate a close relationship with the preexisting Archean granitoids. Zircon from stromatic gneisses and leucosomes ranging in age from 2750 Ma to 2614 Ma produce identical within error $\varepsilon_{Hf}(t)$, and model ages in the range of 3.30 Ga and 3.40 Ga. The model ages are consistent with derivation from a similar magmatic source to that of the Archean gneiss described above and elsewhere in the southern SFC. Although it is absent in the field, the existence of continental crust older than 2.9 Ga is evidenced by the Hf model ages of the detrital zircons, as well as inherited components in a restricted number of gneisses (Hartmann et al., 2006; Lana et al., 2013; Koglin et al., 2014; Moreira et al., 2016; Martínez-Dopico et al., 2017). In addition, Hf model ages for magmatic zircons in gneisses and granitoids from the Bonfim Complex gave values up to 3.0 Ga (Albert et al., 2016). Furthermore, our Hf isotope compositions are consistent with derivation from the host Archean gneisses. As discussed above, the U-Pb and Hf datasets and Sm-Nd T_{DM} model ages obtained by Teixeira et al. (1996) suggest the existence of fragments of Paleoarchean continental crust in the southern SFC that were reworked during the Neoarchean (Lana et al., 2013; Farina et al., 2015; Albert et al., 2016).

Emplacement of large volumes of 2650–2630 Ma high-K syenomonzogranites with negative $\varepsilon Nd_{(t)}$ isotopes have been described in the northern part of the SFC (Cruz et al., 2011; Santos-Pinto et al., 2012; Barbosa et al., 2020; Zincone et al., 2020). Zincone et al. (2020) characterized some of these rocks as depleted in Sr and Ti, enriched in Th, Ba, and Pb, and marked by negative Eu/Eu*. They are interpreted as being derived from crustal reworking of felsic Mesoarchean crust. Other potassic granitoids emplaced in the São Francisco-Congo Craton, mainly those from the nearby Caraguataí, Serra do Eixo and Santa Izabel suites in the Gavião Block (Cruz et al., 2011; Santos-Pinto et al., 2012; Barbosa et al., 2020) bear similar characteristics to those in the south and are possibly linked to the cratonization of the large Archean core of the SFC.

We suggest that the melting of the Archean basement rocks and production of potassic granitoids took place over a ca. 150 Ma period from 2750 Ma to 2600 Ma (Fig. 11). While this is best described in the southern SFC, the partial melting and potassic magmatism seem to be part of a much broader and more extensive event, also involving the segments of the northern (e.g., Zincone et al., 2020) parts of the SFC. This event also includes emplacement of large syenitic intrusions (Cruz et al., 2016) and emplacement of layered mafic–ultramafic intrusions (Teixeira et al., 1998) in the same 2700–2600 Ma interval. The presence of a mafic–ultramafic intrusion in the southern SFC (Teixeira et al., 1998), has long been proposed as evidence for mantle-derived extensional magmatism and partial melting of the lower crust (e.g., Teixeira et al., 1998; Moreno et al., 2017). The heat source for this long-lived period of partial melting and magmatism is likely to have involved mantle sources (e.g., Moreno et al., 2017); however, the crustal signatures recorded in the Hf isotopic composition (e.g., Fig. 9) suggests that the production of the potassic granitoids was dominated by crustal reworking. For instance, large and small batholiths (e.g., Florestal, Mamona, Pequi, Piracema, Samambaia, Souza Nochese; Fig. 1) with well-characterized geochemistry and ages testify to the re-melting of older crustal sources (e.g., Farina et al., 2016; Albert et al., 2016). The broad variation in Hf isotopic composition only confirms an early previous conclusion by Farina et al. (2016) that the source rocks for these granitoids were broadly varied and may have involved sedimentary and metamafic rocks.

6.3. Implications for Late-Archean evolution

Long-lived periods of mid to lower crustal melting and emplacement of large volumes of potassic magmatism form part of an important process of bulk fractionation of the Archean lithosphere (e.g., Romano et al., 2013; Laurent et al., 2014; Farina et al., 2015; Albert et al., 2016; Moyen and Laurent, 2018). Such a process is rooted in the production and mobilization of large volumes of lower crustal melts, which increase the redistribution and transport of heat-producing elements within the crust, and is indirectly responsible for the stabilization of large continental domains (e.g., Romano et al., 2013). As a result, many of the early and late Archean cratons around the world are marked by spikes in potassic granitoids production between 3.0 Ga and 2.5 Ga (e.g., Feng and Kerrich, 1992; Sylvester, 1994; Sage et al., 1996; Champion and Sheraton, 1997; Frost et al., 1998; Champion and Smithies, 1999; Kampunzu et al., 2003; Moyen et al., 2003; Dall'Agnol et al., 2006; Käpyaho et al., 2006; Yang et al., 2008; Schofield et al., 2010; Mikkola et al., 2011).

Compilations by Laurent et al. (2014) point to at least three petrogenetic mechanisms associated with the late Archean granitoids: (a) differentiation of mafic magmas, (b) melting of preexisting crustal rocks, and (c) a combination of magmas produced in the first two processes. However, available petrological, U-Pb and Hf data shows that the bulk of the granitoids generated in the BHC and elsewhere in the SFC crust likely derived from partial melting of the older mafic and felsic crust. Indeed, the enriched isotopic Nd and Hf signatures of late Archean granitoids around the world (e.g., Laurent et al., 2014; Albert et al., 2016) point to widespread reworking between 3.0 Ga and 2.5 Ga and is best reconciled with tectonic accretion of proto-continental masses. This increased development of plate-driven crustal processes from 3.0 Ga (Dhuime et al., 2015) is also reflected in an increased amount of continental detritus into the oceans (e.g., Pons et al., 2013), which here in the SFC can be linked to horizontal lithospheric movements and development of the first accretionary basins between 2800 Ma and 2730 Ma (Moreira et al., 2016).

Recent thermo-mechanical modeling by Chowdhury et al. (2017, 2020) suggests that lithospheric convergence and tectonic

accretions from 3.0 Ga to 2.5 Ga involved large-scale delamination of the lithospheric mantle/lower crust. In this scenario, extensive crustal reworking is expected at various depths as the viscous detachment of the delaminating lithosphere hinders the decoupling between the upper and lower crust, in a process which is called peel back convergence (Chowdhury et al., 2017). The delamination is caused by the upwelling of the warm mantle, which essentially weakens the protocontinental lower crust, promoting extensive melting in the mid to upper crust.

Beneath proto continents such as the SFC, the lithospheric peeling off (or peel back) would contribute to extensive partial melting and felsic magmatism, driven mostly by warmer Archean mantle conditions. Indeed, lower-crustal delamination is invariably regarded as prevalent in the Archean. The significantly higher mantle potential temperatures present during the Archean would enhance the melting of delaminated felsic/mafic crust and produce potassic granitoids with a wide range of compositions. Thus, this embryonic plate tectonic mechanism proposed by Chowdhury et al. (2017) seems a viable mechanism that explains the extended period of partial melting in the SFC, as well as the broad range of partial melting products. The model also reproduces the metamorphic conditions required for partial melting of the earlier crust and links the lithospheric peeling with the peak of potassic granitoid production in Archean cratons. We suggest that this mechanism operated for over 150 million years in the SFC with a continuous and profuse reworking of the older crust and high-temperature metamorphism at shallow depths.

7. Conclusions

Fifteen samples from the Belo Horizonte Complex were dated via LA-ICP-MS. The results reveal a complex and long-lived evolution that spans from 2863 Ma to 2619 Ma. Zircon grains show significantly negative to nearly chondritic initial ε_{Hf} values and model ages from 3.3 Ga to 3.4 Ga, indicating that the rocks from the complex originated from the recycled ancient crust, and suggest the existence of a Paleoarchean crust that encompassed all the basement complexes in the southern part of the SFC. Zircon from the migmatite phases provides evidence that the Archean crust assembled before 2863 Ma and experienced a long and complex history, with significant reworking between 2750 Ma and 2650 Ma. We propose a long-lived period (ca.150 My) of intense partial melting of the southern SFC in the late Archean, similar to what has been recently elucidated from a few other late Archean to early Paleoproterozoic terranes, like the Lewisian Complex (Taylor et al., 2020), the Southern Granulite terrain of India (Chowdhury and Chakraborty, 2019), the Rengali Province (Bose et al., 2021), the Borborema Province (Ferreira et al., 2020) and the Napier Complex of Antarctica (Clark et al., 2018). The partial melting is directly linked to the potassic magmatism that affected whole the SFC between 2750 Ma and 2600 Ma, and has substantially contributed to the stabilization of the Archean lithosphere of the craton.

Declaration of Competing Interest

The authors declare that they have no known competing financial interests or personal relationships that could have appeared to influence the work reported in this paper.

Acknowledgements

This work was possible thanks to financial support from the CNPq (National Council for Scientific and Technological Development) under grant 141707/2016-0 to Lorena Martins, and the financial support provided by CNPq awarded to Cristiano Lana. Ana Alkmim and Débora Vasconcelos are thanked for instrumental tunning during this work. To the Microanalysis Laboratory of the Universidade Federal de Ouro Preto, a member of the Microscopy and Microanalysis Network of Minas Gerais State/Brazil/FAPEMIG, for the CL images.

Appendix A. Supplementary data

Supplementary data to this article can be found online at https://doi.org/10.1016/j.gsf.2021.101289.

References

Aguilar, C., Alkmim, F.F., Lana, C., Farina, F., 2017. Paleoproterozoic assembly of the São Francisco craton, SE Brazil: new insights from U-Pb titanite and monazite dating. Precambrian Res. 289, 95–115.

Albert, C., Farina, F., Lana, C., Stevens, G., Storey, C., Gerdes, A., Martínez Dopico, C., 2016. Archean crustal evolution in the Southern São Francisco craton, Brazil: constraints from U-Pb, Lu-Hf and O isotope analyses. Lithos 266–267, 64–86.

Alkmim, F.F., 2004. O que faz de um cráton um cráton? O Cráton do São Francisco e as revelações Almedianas ao delimita-lo. In: Mantesso-Neto et al. (Eds.), Geologia do Continente Sul-Americano. Evolução da obra de Fernando Flávio Marques de Almeida. Becca, São Paulo, pp.17–35 (in Portuguese with English abstract).

Alkmim, F.F., Marshak, S., 1998. Transamazonian orogeny in the southern São Francisco craton region, Minas Gerais, Brazil: evidence for Paleoproterozoic collision and collapse in the Quadrilátero Ferrífero. Precambrian Res. 90, 29–58.

Alkmim, F.F., Martins-Neto, M.A., 2012. Proterozoic first-order sedimentary sequences of the São Francisco craton, eastern Brazil. Mar. Petrol. Geol. 3, 127–139.

Almeida, F.F.M., Hasui, Y., Brito Neves, B.B., Fuck, R.A., 1981. Brazilian structural provinces: an introduction. Earth-Sci. Rev. 17, 1–29.

Babinski, M., Vieira, L.C., Trindade, R.I.F., 2007. Direct dating of the Sete Lagoas cap carbonate (Bambuí Group, Brazil) and implications for the Neoproterozoic glacial events. Terra Nova 19, 401–406.

Baltazar, O.F., Zucchetti, M., 2007. Lithofacies associations and structural evolution of the Archean Rio das Velhas greenstone belt, Quadrilátero Ferrífero, Brazil: a review of the setting of gold deposits. Ore Geol. Rev. 32, 471–499.

Barbosa, J.S.F., Sabaté, P., 2004. Archean and Paleoproterozoic crust of the São Francisco craton, Bahia, Brazil: geodynamic features. Precambrian Res. 133, 1–27.

Barbosa, N., Teixeira, W., Leal, L.R.B., Leal, A.B.M., 2013. Evolução crustal do setor ocidental do Bloco Arqueano Gavião, Cráton do São Francisco, com base em evidências U-Pb, Sm–Nd e Rb–Sr. Geologia USP. Série Cientifica 13, 63–88 (in Portuguese with English abstract).

Barbosa, R.G., Lana, C.C., Zincone, S.A., 2020. Paleoproterozoic granitic magmatism in the northern São Francisco Craton, NE Brazil: New perspectives from geochemistry, zircon U-Pb geochronology and Hf isotopes. J. S. Am. Earth Sci. 103, 103004.

Bastos-Leal, L.R., Cunha, J.C., Cordani, U.G., Teixeira, W., Nutman, A., Menezes-Leal, A.B., Macambira, M.J.B., 2003. SHRIMP U-Pb, $^{207}Pb/^{206}Pb$ zircon dating and Nd isotopic signature of the Umburanas greenstone belt, Northern São Francisco Craton, Brazil. J. S. Am. Earth Sci. 15, 775–785.

Bauer, A.M., Vervoort, J.D., Fisher, C.M., 2020. Unraveling the complexity of zircons from the 4.0–2.9 Ga Acasta Gneiss Complex. Geochem. Cosmochim. Acta 283, 85–102.

Black, L.P., Gulson, B.L., 1978. The age of the Mud Tank carbonatite, Strangways Range, Northern Territory. J. Aust. Geol. Geophys. 3, 227–232.

Black, L.P., Kamo, S.L., Allen, C.M., Aleinikoff, J.N., Davis, D.W., Korsch, R.J., Foudoulis, C., 2003. TEMORA 1: A new zircon standard for Phanerozoic U-Pb geochronology. Chem. Geol. 200, 155–170.

Blichert-Toft, J., Puchtel, I.S., 2010. Depleted mantle sources through time: evidence from Lu–Hf and Sm–Nd isotope systematics of Archean komatiites. Earth Planet. Sci. Lett. 297 (3–4), 598–606.

Bose, S., Ghosh, G., Kawaguchi, K., Das, K., Mondal, A.K., Banerjee, A., 2021. Zircon and monazite geochronology from the Rengali-Eastern Ghats Province: Implications for the tectonic evolution of the eastern Indian terrane. Precambrian Res. 355, 106080.

Bouvier, A., Vervoort, J.D., Patchett, P.J., 2008. The Lu-Hf and Sm-Nd isotopic composition of CHUR: constraints from unequilibrated chondrites and implications for the bulk composition of terrestrial planets. Earth Planet. Sci. Lett. 273, 48–57.

Campos, J.C.S., Carneiro, M.A., 2008. Neoarchean and Paleoproterozoic granitoids marginal to the Jeceaba-Bom Sucesso lineament (SE border of the southern São Francisco craton): Genesis and tectonic evolution. J. S. Am. Earth Sci. 26, 463–484.

Campos, J.C.S., Carneiro, M.A., Basei, M.A.S., 2003. U-Pb evidence for Late Neoarchean crustal reworking in the southern São Francisco Craton (Minas Gerais, Brazil). An. Acad. Bras. Ciênc. 75 (4), 497–511.

Carneiro, M.A., 1992. O Complexo Metamórfico Bonfim Setentrional (Quadrilátero Ferrífero, Minas Gerais): Litoestratigrafia e evolução geológica de um segmento

de crosta continental do Arqueano. Unpublished Ph.D. Thesis, Universidade de São Paulo, 233 pp.
Carneiro, M.A., Jordt-Evangelista, H., Teixeira, W., 1997. Eventos magmáticos arqueanos de natureza cálcio-alcalina e tholeíitica no Quadrilátero Ferrífero e suas implicações tectônicas. Rev. Bras. Geociênc. 27, 121–128.
Carvalho, B.B., Sawyer, E.W., Janasi, V.A., 2016. Crustal reworking in a shear zone: transformation of metagranite to migmatite. J. Metamorph. Geol. 34, 237–264.
Carvalho, B.B., Janasi, V.A., Sawyer, E.W., 2017. Evidence for Paleoproterozoic anatexis and crustal reworking of Archean crust in the São Francisco Craton, Brazil: a dating and isotopic study of the Kinawa migmatite. Precambrian Res. 291, 98–118.
Champion, D.C., Sheraton, J.W., 1997. Geochemistry and Nd isotope systematics of Archaean granites of the Eastern Goldfields, Yilgarn Craton, Australia: implications for crustal growth processes. Precambrian Res. 83 (1–3), 109–132.
Champion, D.C., Smithies, R.H., 1999. Archaean granites of the Yilgarn and Pilbara cratons, Western Australia: secular changes. In: Barbarin, B. (Ed.), The Origin of Granites and Related Rocks—IVth Hutton Symposium Abstracts Doc. BRGM 290, pp. 134-137.
Chemale, F., Babinski, M., Van Schmus, W.R., 1993. U/Pb dating of granitic–gneissic rocks from the Belo Horizonte and Bonfim complexes, Quadrilátero Ferrífero (Brazil). In: Report for CNPq and NSFEAR Project on São Francisco Craton Margin Transect Project, p. 16.
Chowdhury, P., Chakraborty, S., 2019. Slow cooling at higher temperatures recorded within high-P mafic granulites from the Southern Granulite Terrain, India: implications for the presence and style of plate tectonics near the Archean-Proterozoic boundary. J. Petrol. 60, 441–486.
Chowdhury, P., Gerya, T., Chakraborty, S., 2017. Emergence of silicic continents as the lower crust peels off on a hot plate-tectonic Earth. Nat. Geosci. 10, 698–703.
Chowdhury, P., Chakraborty, P., Gerya, T.V., Cawood, P.A., Capitanio, F.A., 2020. Peel-back controlled lithospheric convergence explains the secular transitions in Archean metamorphism and magmatism. Earth Planet. Sci. Lett. 538, 116224.
Chu, N.C., Taylor, R.N., Chavagnac, V., Nesbitt, R.W., Boella, R.M., Milton, J.A., German, C.R., Bayon, G., Burton, K., 2002. Hf isotope ratio analysis using multi-collector inductively coupled plasma mass spectrometry: an evaluation of isobaric interference corrections. J. Anal. Atom. Spectrom. 17, 1567–1574.
Claesson, S., Bibikova, E.V., Shumlyanskyy, L., Whitehouse, M.J., Billström, K., 2016. Can oxygen isotopes in magmatic zircon be modified by metamorphism? A case study from the Eoarchean Dniester-Bug Series, Ukrainian Shield. Precambrian Res. 273, 1–11.
Clark, C., Taylor, R.J.M., Kylander-Clark, A.R.C., Hacker, B.R., 2018. Prolonged (>100 Ma) ultrahigh temperature metamorphism in the Napier Complex, East Antarctica: a petrochronological investigation of Earth's hottest crust. J. Metamorph. Geol. 36, 1117–1139.
Corfu, F., Ayres, L.D., 1984. U-Pb ages and genetic significance of heterogeneous zircon populations in rocks from the Favourable Lake area, northwestern Ontario. Contrib. Mineral. Petr. 88, 86–101.
Corfu, F., Hanchar, J.M., Hoskin, P.W.O., Kinny, P., 2003. Atlas of zircon textures. Rev. Mineral. Geochem 53, 469–500.
Crowley, Q.G., Heron, K., Riggs, N., Kamber, B., Chew, D., McConnell, B., Benn, K., 2014. Chemical abrasion applied to LA-ICP-MS U-Pb zircon geochronology. Fortschr. Mineral. 4, 503–518.
Cruz, S.C.P., Peaucat, J.J., Teixeira, L., Carneiro, M.A., Martins, A.A.M., Santana, J.S.S., Souza, J.S., Barbosa, J.S.F., Leal, A.B.M., Dantas, E., Pimentel, M., 2011. The Caraguataí syenitic suite, a ca. 2.7 Ga-old alkaline magmatism (petrology, geochemistry and U/Pb zircon ages). Southern Gavião block (São Francisco Craton), Brazil. J. S. Am. Earth Sci. 37, 95–112.
Cruz, S.C.P., Barbosa, J.S.F., Pinto, M.S., Peucat, J.-J., Paquette, Souza, J.S., Martins, V.S., Chemale Jr, F., Carneiro, M.A., 2016. The Siderian-Orosirian magmatism in the Gavião Paleoplate, Brazil: U-Pb geochronology, geochemistry and tectonic implications. J. S. Am. Earth Sci. 69, 43–79.
Cutts, K., Lana, C.C., Alkmim, F.F.A., Farina, F., Moreira, H.S., Coelho, V., 2019. Metamorphism and exhumation of basement gneiss domes in the Quadrilátero Ferrífero: Two stage dome-and-keel evolution? Geosci. Front. 10, 1765–1787.
Dall'Agnol, R., Oliveira, M.A., Almeida, J.A.C., Althoff, F.J., Leite, A.A.S., Oliveira, D.C., Barros, C.E.M., 2006. Archean and Paleoproterozoic granitoids of the Carajás metallogenetic province, eastern Amazonian craton. In: Dall'Agnol, R., Rosa-Costa, L.T., Klein, E.L. (Eds.), Symposium on Magmatism.: Crustal Evolution, and Metallogenesis of the Amazonian Craton. Abstracts Volume and Field Trips Guide. Belém, PRONEX-UFPA/SBGNO. PRONEX-UFPA/SBGNO, Belém, pp. 99–150.
Dhuime, B., Wuestefeld, A., Hawkesworth, C.J., 2015. Emergence of modern continental crust about 3 billion years ago. Nat. Geosci. 8, 552–555.
Dorr II, J.V.N., 1969. Physiographic, stratigraphic and structural development of the Quadrilátero Ferrífero, Minas Gerais, Brazil. U.S. Geol. Surv. Prof. Paper 641-A, 1–110.
Farina, F., Albert, C., Lana, C., 2015. The Neoarchean transition between medium- and high-K granitoids: clues from the southern São Francisco craton (Brazil). Precambrian Res. 266, 375–394.
Farina, F., Albert, C., Martinez-Dopico, C., Aguilar Gil, C., Moreira, H., Hippertt, J., Cutts, K., Lana, C., Alkmim, F.F., 2016. The Archean-Paleoproterozoic evolution of the Quadrilátero Ferrífero (Brasil): current models and open questions. J. S. Am. Earth Sci. 68, 4–21.
Feng, R., Kerrich, R., 1992. Geochemical evolution of granitoids from the Archean Abitibi Southern Volcanic Zone and the Pontiac subprovince, Superior Province, Canada: implications for tectonic history and source regions. Chem. Geol. 98, 23–70.
Ferreira, A.C.D., Dantas, E.L., Fuck, R.A., Nedel, I.M., 2020. Arc accretion and crustal reworking from late Archean to Neoproterozoic in Northeast Brazil. Sci. Rep. 10, 7855.
Frost, C.D., Frost, B.R., Chamberlain, K.R., Huselbosch, T.P., 1998. The Late Archaean history of the Wyoming province as recorded by granitic magmatism in the Wind River Range, Wyoming. Precambrian Res. 98, 145–173.
Geisler, T., Schaltegger, U., Tomaschek, F., 2007. Re-equilibration of zircon in aqueous fluids and melts. Elements 3, 43–50.
Gerdes, A., Zeh, A., 2006. Combined U-Pb and Hf isotope LA-(MC)-ICP-MS analyses of detrital zircons: comparison with SHRIMP and new constraints for the provenance and age of an Armorican metasediment in Central Germany. Earth Planet. Sci. Lett. 249, 47–61.
Gerdes, A., Zeh, A., 2009. Zircon formation versus zircon alteration—New insights from combined U-Pb and Lu–Hf in-situ LA-ICP-MS analyses, and consequences for the interpretation of Archean zircon from the Central Zone of the Limpopo Belt. Chem. Geol. 261, 230–243.
Goulart, L.E.A., Carneiro, M.A., Endo, I., Suita, M.T.F., 2013. New evidence of Neoarchean crustal growth in southern São Francisco Craton: the Carmópolis de Minas Layered Suite, Minas Gerais, Brazil. Braz. J. Geol. 43, 445–459.
Griffin, W.L., Pearson, N.J., Belousova, E., Jackson, S.V., Van Achterbergh, E., O'Reilly, S.Y., Shee, S.R., 2000. The Hf isotope composition of cratonic mantle: LAM-MC-ICPMS analysis of zircon megacrysts in kimberlites. Geochim. Cosmochim. Acta 64, 133–147.
Hartmann, L.A., Endo, I., Suita, M.T.F., Santos, J.O.S., Frantz, J.C., Carneiro, M.A., McNaughton, N.J., Barley, M.E., 2006. Provenance and age delimitation of Quadrilátero Ferrífero sandstone based on zircon U-Pb isotopes. J. S. Am. Earth Sci. 20, 273–285.
Heilbron, H., Cordani, U., Alkmim, F., Reis, H., 2017. Tectonic genealogy of a miniature continent. In: Heilbron, M., Cordani, U.G., Alkmim, F.F. (Eds.), São Francisco Craton, Eastern Brazil. Regional Geology Reviews. Springer, Cham, pp. 321–331.
Herz, N., 1970. Gneissic and igneous rocks of the Quadrilátero Ferrífero, Minas Gerais, Brazil. U.S. Geol. Surv. Prof. Paper 641-B, B1–B58.
Hoskin, P.W.O., Black, L.P., 2000. Metamorphic zircon formation by solid-state recrystallization of protolith igneous zircon. J. Metamorph. Geol. 18, 423–439.
Huyskens, M.H., Zink, S., Amelin, Y., 2016. Evaluation of temperature-time conditions for the chemical abrasion treatment of single zircons for U-Pb geochronology. Chem. Geol. 438, 25–35.
Jackson, S.E., Pearson, N.J., Griffin, W.L., Belousova, E.A., 2004. The application of laser ablation-inductively coupled plasma-mass spectrometry to in situ U-Pb zircon geochronology. Chem. Geol. 211, 47–69.
Kampunzu, A.B., Tombale, A.R., Zhai, M., Bagai, Z., Majaule, T., Modisi, M.P., 2003. Major and trace element geochemistry of plutonic rocks from Francistown, NE Botswana: evidence for a Neoarchean continental active margin in the Zimbabwe craton. Lithos 71, 431–460.
Käpyaho, A., Mänttäri, I., Huhma, H., 2006. Growth of Archaean crust in the Kuhmo district, Eastern Finland: U-Pb and Sm–Nd isotope constraints on plutonic rocks. Precambrian Res. 146, 95–119.
Koglin, N., Zeh, A., Cabral, A.R., Gomes Jr., A.A.S., Neto, A.V.C., Brunetto, W.J., Galbiatti, H., 2014. Depositional age and sediment source of the auriferous Moeda Formation, Quadrilátero Ferrífero of Minas Gerais Brazil: new constraints from U-Pb–Hf isotopes in zircon and xenotime. Precambrian Res. 255, 96–108.
Lana, C., Alkmim, F.F., Armstrong, R., Scholz, R., Romano, R., Nalini, H.A., 2013. The ancestry and magmatic evolution of Archaean TTG rocks of the Quadrilátero Ferrífero province, southeast Brazil. Precambrian Res. 230, 1–30.
Laurent, O., Martin, H., Moyen, J.F., Doucelance, R., 2014. The diversity and evolution of late-Archean granitoids: evidence for the onset of "modern-style" plate tectonics between 3.0 and 2.5 Ga. Lithos 205, 208–235.
Ledru, P., Johan, V., Milesi, J.P., Tegyey, M., 1994. Evidence for a 2 Ga continental accretion in the circum-south Atlantic provinces. Precambrian Res. 69, 169–191.
Ludwig, K.R., 2012. Isoplot Version 3.75: a Geochronological Toolkit for Microsoft Excel. Berkeley Geochronology Center, Berkeley, CA, p.75.
Machado, N., Carneiro, M.A., 1992. U-Pb evidence of the late Archean tectono-thermal activity in the southern São Francisco shield, Brazil. Can. J. Earth Sci. 29, 2341–2346.
Machado, N., Noce, C.M., Ladeira, E.A., de Oliveira, O.A.B., 1992. U-Pb geochronology of the Archean magmatism and Proterozoic metamorphism in the Quadrilátero Ferrífero, southern São Francisco craton, Brazil. Geol. Soc. Am. Bull. 104, 1221–1227.
Machado, N., Schrank, A., Noce, C.M., Gauthier, G., 1996. Ages of detrital zircon from Archean-Paleoproterozoic sequences: implications for Greenstone Belt setting evolution of a Transamazonian foreland basin in Quadrilátero Ferrífero, southeast Brazil. Earth Planet. Sci. Lett. 141, 259–276.
Martínez-Dopico, C.I., Lana, C., Moreira, H.S., Cassino, L.F., Alkmim, F.F., 2017. U-Pb ages and Hf-isotope data of detrital zircons from the late Neoarchean-Paleoproterozoic Minas Basin, SE Brazil. Precambrian Res. 291, 143–161.
Mattinson, J.M., 2005. Zircon U-Pb chemical abrasion ("CA-TIMS") method: combined annealing and multi-step partial dissolution analysis for improved precision and accuracy of zircon ages. Chem. Geol. 220 (1–2), 47–66.
Mikkola, P., Huhma, H., Heilimo, E., Whitehouse, M., 2011. Archean crustal evolution of the Suomussalmi district as part of the Kianta Complex, Karelia: constraints from geochemistry and isotopes of granitoids. Lithos 125, 287–307.

Moreira, H., Lana, C., Nalini Jr., H.N., 2016. The detrital zircon record of an Archaean convergent basin in the Southern São Francisco Craton, Brazil. Precambrian Res. 275, 84–99.
Morel, M.L.A., Nebel, O., Nebel-Jacobsen, Y.J., Miller, J.S., Vroon, P.Z., 2008. Hafnium isotope characterization of the GJ-1 zircon reference material by solution and laser-ablation MC-ICPMS. Chem. Geol. 255, 231–235.
Moreno, J.A., Baldim, M.R., Semprich, J., Oliveira, E.P., Verma, S.K., Teixeira, W., 2017. Geochronological and geochemical evidences for extension-related Neoarchean granitoids in the southern São Francisco Craton, Brazil. Precambrian Res. 294, 322–343.
Moyen, J.F., Martin, H., Jayananda, M., Auvray, B., 2003. Late Archaean granites: a typology based on the Dharwar Craton (India). Precambrian Res. 127, 103–123.
Moyen, J.F., Laurent, O., 2018. Archaean tectonic systems: a view from igneous rocks. Lithos 302, 99–125.
Nebel, O., Capitanio, F.A., Moyen, J.F., Weinberg, R.F., Clos, F., Nebel-Jacobsen, Y.J., Cawood, P.A., 2018. When crust comes of age: on the chemical evolution of Archaean, felsic continental crust by crustal drip tectonics. Philos. Trans. -Royal Soc. A, Math. Phys. Eng. Sci. 376 (2132), 20180103.
Noce, C.M., 1995. Geocronologia dos eventos magmáticos, sedimentares e metamórficos na região do Quadrilátero Ferrífero, Minas Gerais Unpublished Ph.D. Thesis. Universidade de São Paulo, p. 129 pp..
Noce, C.M., Machado, N., Teixeira, W., 1998. U-Pb geochronology of gneisses and granitoids in the Quadrilátero Ferrífero (southern São Francisco craton): age constraints for Archean and Paleoproterozoic magmatism and metamorphism. Rev. Bras. Geociênc. 28, 95–102.
Noce, C.M., Teixeira, W., Quemeneur, J.J.G., Martins, V.T.S., Bolzachini, E., 2000. Isotopic signatures of Paleoproterozoic granitoids from the southern São Francisco craton and implications for the evolution of the Transamazonian orogeny. J. S. Am. Earth Sci. 13, 225–239.
Noce, C.M., Zuccheti, M., Baltazar, O.F., Armstrong, R., Dantas, E., Renger, F.E., Lobato, L.M., 2005. Age of felsic volcanism and the role of ancient continental crust in the evolution of the Neoarchean Rio das Velhas greenstone belt (Quadrilátero Ferrífero, Brazil): U-Pb zircon dating of volcaniclastic graywackes. Precambrian Res. 141, 67–82.
Oliveira, A.H., 2004. Evolução tectônica de um fragmento do Cráton São Francisco Meridional com base em aspectos estruturais, geoquímicos (rocha total) e geocronológicos (Rb–Sr, Sm–Nd, Ar–Ar, U–Pb). Ph.D. Thesis, Universidade Federal de Ouro Preto, 136pp.
Oliveira, E.P., Windley, B.F., Araújo, M.N.C., 2010. The Neoproterozoic Sergipano orogenic belt, NE Brazil: a complete plate tectonic cycle in western Gondwana. Precambrian Res. 181, 64–84.
Oliveira, E.P., McNaughton, N.J., Zincone, S.A., Talavera, C., 2020. Birthplace of the São Francisco Craton, Brazil: Evidence from 3.60 to 3.64 Ga Gneisses of the Mairi Gneiss Complex. Terra Nova 32, 281–289.
Pons, M.L., Fujii, T., Rosing, M., Quitté, G., Télouk, P., Albarède, F., 2013. A Zn isotope perspective on the rise of continents. Geobiology 11, 201–214.
Romano, A.W., 1989. Evolution tectonique de la région NW du Quadrilatère Ferrifère – Minas Gerais, Brésil Unpublished Ph.D. Thesis. University of Nancy, France, p. 259.
Romano, R., Lana, C., Alkmim, F.F., Stevens, G., Armstrong, R., 2013. Stabilization of the Southern São Francisco Craton, SE Brazil, through a long-lived and episodic period of potassic magmatism. Precambrian Res. 224, 1–20.
Sage, R.P., Lightfoot, P.C., Doherty, W., 1996. Geochemical characteristics of granitoid rocks from within the Archean Michipicoten Greenstone Belt, Wawa Subprovince, Superior Province, Canada: implications for source regions and tectonic evolution. Precambrian Res. 76, 155–190.
Santos, M.M., Lana, C., Scholz, R., Buick, I., Schmitz, M.D., Kamo, S.L., Gerdes, A., Corfu, F., Tapster, S., Lancaster, P., Storey, C.D., Basei, M.A.S., Tohver, E., Alkmim, A., Nalini, H., Krambrock, K., Fantini, C., 2017. A new appraisal of Sri Lankan zircons as reference material for in situ U-Pb geochronology, REE analyses and Lu-Hf isotope tracing. Geostand. Geoanal. Res. 41, 335–358.
Santos-Pinto, M.A.S., Peucat, J.J., Martin, H., Barbosa, J.S.F., Fanning, C.M., Cocherie, A., Paquette, J.L., 2012. Crustal evolution between 2.0 and 3.5 Ga in the southern Gavião block (Umburanas-Brumado-Aracatu region), São Francisco Craton, Brazil: a 3.5–3.8 Ga proto-crust in the Gavião block? J. S. Am. Earth Sci. 40, 129–142.
Scherer, E., Münker, C., Mezger, K., 2001. Calibration of the lutetium–hafnium clock. Science 293, 683–686.
Schofield, D.I., Thomas, R.J., Goodenough, K.M., de Waele, B., Pitfield, P.E.J., Key, R.M., Bauer, W., Walsg, G.J., Lidke, D.J., Ralison, A.V., Rabarimanana, M., Rafahatelo, J. M., Randriamananjara, T., 2010. Geological evolution of the Antogil Craton, NE Madagascar. Precambrian Res. 182, 187–203.
Schrank, A., Machado, N., 1996. Idades U-Pb em monazitas e zircões do distrito aurífero de Caeté, da Mina de Cuiabá e do Depósito de Carrapato, Quadrilátero Ferrífero (MG). Anais 39th Congr. Bras. Geol., Salvador, Soc. Bras. Geol. v. 6, p. 473–475.
Silva, L.C., Pedrosa-Soares, A.C., Dussin, I., Armstrong, R.., Noce, C.M., 2012 a. O Complexo Belo Horizonte de Carlos Noce revisitado. Open file (ppt) report, http://www.46cbg.com.br/0110/sala3/10h10_luiz_carlos_01-10_sl03.ppt.pdf.
Simon, M.B., Bongiolo, E.M., Ávila, C.A., Oliveira, E.P., Teixeira, W., Stohler, R.C., Soares de Oliveira, F.V., 2018. Neoarchean reworking of TTG-like crust in the southernmost portion of the Sao Francisco Craton: U-Pb zircon dating and geochemical evidence from the Sao Tiago Batholith. Precambrian Res. 314, 353–376.
Sláma, J., Košler, J., Condon, D.J., Crowley, J.L., Gerdes, A., Hanchar, J.M., Horstwood, M.S.A., Morris, G.A., Nasdala, L., Norberg, N., Schaltegger, U., Schoene, B., Tubrett, M.N., Whitehouse, M.J., 2008. Plešovice zircon – a new natural reference material for U-Pb and Hf isotopic microanalysis. Chem. Geol. 249, 1–35.
Söderlund, U., Patchett, P.J., Vervoort, J.D., Isachsen, C.E., 2004. The 176Lu decay constant determined by Lu–Hf and U-Pb isotope systematics of Precambrian mafic intrusions. Earth Planet. Sci. Lett. 219, 311–324.
Sylvester, P.J., 1994. Archaean granite plutons. In: Condie, K.C. (Ed.), Archaean Crustal Evolution. Developments in Precambrian Geology, vol. 11. Elsevier, Amsterdam, pp. 261–314.
Taylor, S.R., McLennan, S.M., 1995. The geochemical evolution of the continental crust. Rev. Geophys. 33, 241–265.
Taylor, R.J.M., Johnson, T.E., Clark, C., Harrison, R.J., 2020. Persistence of melt-bearing Archean lower crust for >200 m.y.—an example from the Lewisian Complex northwest Scotland. Geology 48, 221–225.
Teixeira, W., Caneiro, M.A., Noce, C.M., Machado, N., Sato, K., Taylor, P.N., 1996. Pb, Sr and Nd isotope constraints on the Archaean evolution of gneissic-granitoid complexes in the southern São Francisco Craton, Brazil. Precambrian Res. 78, 151–164.
Teixeira, W., Cordani, U.G., Nutman, A.P., Sato, K., 1998. Polyphase Archean evolution in the Campo Belo metamorphic Complex, Southern São Francisco Craton, Brazil: SHRIMP U-Pb zircon evidence. J. S. Am. Earth Sci. 11 (3), 279–289.
Teixeira, W., Figueiredo, M.C.H., 1991. An outline of Early Proterozoic crustal evolution in the Sao Francisco craton, Brazil: a review. Precambrian Res. 53, 1–22.
Teixeira, W., Sabaté, P., Barbosa, J., Noce, C.M., Carneiro, M.A., 2000. Archean and Paleoproterozoic tectonic evolution of the São Francisco Craton. In: Cordani UG, Milani EJ, Thomaz-Filho A, Campos DA (Eds.), Tectonic Evolution of South America. 31st IGC, pp. 101–137.
Van Achterbergh, E., Ryan, C.G., Jackson, S.E., Griffin, W.L., 2001. Data reduction software for LA-ICP-MS: appendix. Assoc. Canada (MAC) Short Course Series 29, p. 239.
Wedepohl, K.H., 1995. The composition of the continental crust. Geochem. Cosmochim. Ac. 59 (1), 217–239.
Wiedenbeck, M., Allé, P., Corfu, F., Griffin, W.L., Meier, M., Oberli, F., von Quadt, A., Roddick, J.C., Spiegel, W., 1995. Three natural zircon standards for U-Th-Pb, Lu-Hf, trace element and REE analyses. Geostandard Newslett. 19, 1–23.
Wiedenbeck, M., Hanchar, J.M., Peck, W.H., Sylvester, P., Valley, J.W., Whitehouse, M.J., Kronz, A., Morishita, Y., Nasdala, L., Fiebig, J., Franch,i I., Girard, J.P., Greenwood, R.C., Hinton, R., Kita N., Mason, P.R.D., Norman, M., Ogasawara, M., Piccoli, R., Rhede, D., Satoh, H., Schulz-Dobrick, B., Skar, O., Spicuzza, M.J., Terada, K., Tindle, A., Togashi, S., Vennemann, T., Xie, Q., Zheng, Y.F., 2004. Further characterisation of the 91500 zircon crystal. Geostand. Geoanal. Res. 28, 9–39.
Wiedmann, P., Davies, J.H.F.L., Schaltegger, U., 2019. Calibrating chemical abrasion: Its effects on zircon crystal structure, chemical composition and U-Pb age. Chem. Geol. 511, 1–10.
Wiemer, D., Allen, C., Murphy, D., Kinaev, I., 2017. Effects of thermal annealing and chemical abrasion on ca. 3.5 Ga metamict zircon and evidence for natural reverse discordance: Insights for U-Pb LA-ICP-MS dating. Chem. Geol. 466, 285–302.
Woodhead, J.D., Hergt, J.M., 2005. A preliminary appraisal of seven natural zircon reference materials for in situ Hf isotope determination. Geostand. Geoanal. Res. 29, 183–195.
Xia, Q.X., Zheng, Y.F., Yuan, H., Wu, F.Y., 2009. Contrasting Lu–Hf and U-Th–Pb isotope systematics between metamorphic growth and recrystallization of zircon from eclogite-facies metagranites in the Dabie orogen, China. Lithos 112, 477–496.
Yang, J.H., Wu, F.Y., Wilde, S.A., Zhao, G., 2008. Petrogenesis and geodynamics of Late-Archaean magmatism in eastern Hebei, eastern North China Craton: geochronological, geochemical and Nd–Hf isotopic evidence. Precambrian Res. 167, 125–149.
Zincone, S.A., Oliveira, E.P., Ribeiro, B.P., Marinho, M.M., 2020. High-K granites between the Archean Gavião and Jequié blocks, São Francisco Craton, Brazil: Implications for cratonization and amalgamation of the Rhyacian Atlantica continent. J. S. Am. Earth Sci. 103, 102920.